Copyright Warning & Restrictions

The copyright law of the United States (Title 17, United States Code) governs the making of photocopies or other reproductions of copyrighted material.

Under certain conditions specified in the law, libraries and archives are authorized to furnish a photocopy or other reproduction. One of these specified conditions is that the photocopy or reproduction is not to be "used for any purpose other than private study, scholarship, or research." If a, user makes a request for, or later uses, a photocopy or reproduction for purposes in excess of "fair use" that user may be liable for copyright infringement,

This institution reserves the right to refuse to accept a copying order if, in its judgment, fulfillment of the order would involve violation of copyright law.

Please Note: The author retains the copyright while the New Jersey Institute of Technology reserves the right to distribute this thesis or dissertation

Printing note: If you do not wish to print this page, then select "Pages from: first page # to: last page #" on the print dialog screen

ABSTRACT

SEQUENTIAL BAYESIAN FILTERING FOR SPATIAL ARRIVAL TIME ESTIMATION

by
Rashi Jain

Locating and tracking a source in an ocean environment as well as estimating environmental parameters of a sound propagation medium is of utmost importance in underwater acoustics. Matched field processing is often the method of choice for the estimation of such parameters. This approach, based on full field calculations, is computationally intensive and sensitive to assumptions on the structure of the environment. As an alternative, methods that use only select features of the acoustic field for source localization and environmental inversion have been proposed. The focus here is on inversion using arrival times of identified paths within recorded time-series. After a short study of a linearization techniques employing such features and numerical issues on their implementation, we turn our attention to the need for accurate extraction of arrival times for accurate estimation. We develop a particle filtering approach that treats arrival times as "targets", dynamically modeling their "location" at arrays of spatially separated receivers. Using Monte Carlo simulations, we perform an evaluation of our method and compare it to conventional Maximum Likelihood (ML) estimation. The comparison demonstrates an advantage in using the proposed approach, which can be employed as a pre-inversion tool for minimization and quantification of uncertainty in arrival time estimation.

SEQUENTIAL BAYESIAN FILTERING FOR SPATIAL ARRIVAL TIME ESTIMATION

by
Rashi Jain

A Dissertation
Submitted to the Faculty of
New Jersey Institute of Technology and
Rutgers, The State University of New Jersey – Newark
in Partial Fulfillment of the Requirements for the Degree of
Doctor of Philosophy in Mathematical Sciences

Department of Mathematical Sciences, NJIT
Department of Mathematics and Computer Science, Rutgers-Newark

May 2011

APPROVAL PAGE

SEQUENTIAL BAYESIAN FILTERING FOR SPATIAL ARRIVAL TIME ESTIMATION

Rashi Jain

Dr. Zoi-Heleni Michalopoulou, Dissertation Advisor — Date
Professor, Department of Mathematical Sciences, New Jersey Institute of Technology

---

Dr. Ali Abdi, Committee Member — Date
Associate Professor,Department of Electrical Engineering, New Jersey Institute of Technology

---

Dr. Manish Bhattacharjee, Committee Member — Date
Professor, Department of Mathematical Sciences, New Jersey Institute of Technology

---

Dr. Sunil Dhar, Committee Member — Date
Associate Professor, Department of Mathematical Sciences, New Jersey Institute of Technology

---

Dr. Jonathan Luke, Committee Member — Date
Professor, Department of Mathematical Sciences, New Jersey Institute of Technology

BIOGRAPHICAL SKETCH

Author: Rashi Jain

Degree: Doctor of Philosophy

Date: May 2011

Undergraduate and Graduate Education:

- Doctor of Philosophy in Mathematical Sciences,
  New Jersey Institute of Technology, Newark, NJ, 2011
- Master of Science in Applied Mathematics
  New Jersey Institute of Technology, Newark, NJ, 2008
- Master of Science in Mathematics,
  Indian Institute of Technology, Delhi, India 2003

Major: Mathematical Sciences

Presentations and Publications:

Rashi Jain and Zoi-Heleni Michalopoulou, "Particle filtering for sequential multipath arrival time and amplitude estimation," *Invited Paper*, Journal of the Acoustical Society of America, vol. 127, 2010.

Rashi Jain and Zoi-Heleni Michalopoulou, "A particle filtering approach for multipath arrival time estimation from acoustic time series," Journal of the Acoustical Society of America, vol. 126, 2009.

Rashi Jain and Zoi-Heleni Michalopoulou, "Arrival Time Estimation from Sound Signals in the Ocean: Particle Filtering Approach," *Journal of the Acoustical Society of America*, vol. 124, 2008.

Rashi Jain and Zoi-Heleni Michalopoulou, "Robust source localization and geoacoustic inversion in the Haro Strait Primer," *Journal of the Acoustical Society of America*, vol. 120, 2006.

This work is dedicated to my parents, family and friends who always believed in me and supported me during the toughest phases. The journey of life is a continuous learning process and it is in following words that I can describe my lesson:

"You cannot control what happens to you, but you can control your attitude toward what happens to you, and in that, you will be mastering change rather than allowing it to master you" -Sri Ram

Rashi

ACKNOWLEDGMENT

I am heartily thankful to my supervisor, Dr. Eliza Michalopoulou, whose supervision, guidance and support, provided immense help towards the completion of this research work. I will also like to offer my gratitude to the ONR (Office of Naval Research) whose sponsorship [ONR grant number: N00014-07-1-0521] facilitated the progress of this research and to all my committee members for their time, valuable suggestions and support through the course of this work.

TABLE OF CONTENTS

Chapter **Page**

TABLE OF CONTENTS
(Continued)

Chapter **Page**

LIST OF TABLES

Table **Page**

LIST OF FIGURES

LIST OF FIGURES
(Continued)

Figure **Page**

LIST OF FIGURES
(Continued)

Figure **Page**

CHAPTER 1

INTRODUCTION

1.1 Motivation

The problem of locating and tracking a single or multiple acoustic sources in a multipath environment is of interest in many areas. In underwater applications, estimating the time evolution of a target's position from noise corrupted signal measurements at arrays of hydrophones is an important problem for defense purposes or environmental surveys. Other areas where such problems frequently appear include speech recognition, seismology, and robotics, where specific applications might include automatic camera steering for video-conferencing, identification of individual speakers in multi-source environments, information on steering for microphone arrays, and autonomous naviga- tion for robots.

Motivated by the importance of environmental parameter estimation and localization of a sound source in the ocean, we focus on the problem of accurately estimating arrival times and amplitudes of acoustic signals arriving at an array of receivers in an underwater waveguide. Arrival time and amplitude estimates can provide in an efficient manner information on source location and ocean properties such as water column depth, speed of sound propagation, and sediment attenuation, knowledge of which is valuable for ocean exploration and advanced sonar design.

1.2 Problem Description

An array of spatially separated receivers is placed in a shallow water environment and acoustic signals are received from a source placed at some distance from the array of hydrophones. The main objective in the beginning of our study is to acoustically determine the geometry of propagation and some environmental properties of the medium, and later on, our objective is to accurately determine ray arrival times and

amplitudes for distinct rays identified at the array of receivers. The aim is to formulate our parameter estimation problem in a nonlinear tracking-smoothing framework, in order to obtain accurate travel time and amplitude estimates to be used for robust localization and environmental inversion. Arrival times and amplitudes of additional paths are then calculated from both synthetic and real data.

1.3 Background

In underwater acoustics, several methods have been presented for source localization, geoacoustic inversion, and tracking. The task of acoustic source localization in a shallow water environment is challenging because of the noise interference from sources present in coastal and the inadequately understood propagation environment. Matched field processing (MFP) is a method frequently used for source localization in the ocean [1, 2, 3, 4, 5]. MFP employs a sound propagation model for the calculation of full acoustic fields, known as replicas, that are then correlated to the received field at an array of phones [5, 6, 7, 8, 9]. The values generating the best match (highest correlation) between the true and replica fields are the estimates of the unknown parameters. Various forms of MFP have been proposed; the most widely used one is the Bartlett processor, which calculates the inner product between the received data and normalized replica fields.

To successfully compute the parameters of interest, one must make certain assumptions regarding sound propagation. Uncertainties on factors such as water column depth, receiver depth, receiver ranges, and bottom sediment properties must be incorporated in the estimation process to ensure accurate results, resulting in a complex, highly non-linear, and comp problem.

In order to overcome this problem, linearized inversion [10, 11] has been proposed for source localization and inversion for sediment related quantities, such as sound speed and layer thickness. The method uses arrival times estimated from

signals received at an array of phones. At the same time, replica arrival times are computed using an assumed geometry and environment and are then compared to estimated arrival times. Accurate estimation of arrival times from the received signals is required for this method to perform well.

In a multipath environment, the job of detecting peaks and associating them to the right ray paths is difficult; that is, data-association is complex, because one does not know which peak corresponds to which arrival. Thus, selection of an appropriate arrival time (or time delay) estimation method is crucial. Many algorithms have been developed for arrival time estimation [12, 13, 14], including a simple cross-correlation of the received and source signals [15, 16, 17]. Maximum a Posteriori (MAP) estimation has also been proposed [18]. With this method, estimation of the unknown parameters is obtained by maximizing the posterior probability density function (PDF) of the unknown parameters given prior knowledge and received data. MAP estimation has an excellent performance but is computationally expensive since it conventionally requires exhaustive calculation of the posterior distribution of the parameters. An approach known as the Gibbs Sampling Maximum A Posteriori (GS-MAP), was proposed in [19], which combines both the MAP framework and a fast Gibbs sampler [20, 21] for the efficient computation of the posterior joint PDF of all unknown parameters at every phone. The shortcoming of this method is its inability to tie information across different receivers. This has sparked our interest in developing sequential Bayesian methods for more comprehensive and accurate arrival time estimation.

1.4 Research Focus and Thesis Structure

In our research, we first estimate parameters such as source and receiver range and depth and water column depth using linearized inversion and regularization. The aim is to generalize the approach developed in [10, 11, 19] by introducing a sloping

ocean bottom in the geometry of the ocean environment, more closely representing true environmental conditions. The arrival times employed in the work are estimated with the GS-MAP approach, which jointly estimates number of arriving paths, their arrival times and amplitudes, and the noise level. We show with real data, that our approach, integrating a more accurate description of the environment in the inversion process in comparison to other methods, produces estimates that are closer to ground truth data. This work is presented in Chapter 2.

Since inversion quality depends on the accuracy in arrival time extraction, we subsequently work on improving arrival time estimates. The idea we decided to explore was to employ information on arrival times from one receiver to the next to improve arrival time estimation at each phone. This direction of using information from one hydrophone for the estimation process at another hydrophone leads us to the concept of sequential Bayesian filtering. Since Bayesian filters have the power to exploit the correlation of motion of a target from one window to another [22, 23], it is possible to estimate parameters such as arrival times more tightly when we exploit spatial information rather than than by only employing data at a single phone. Specifically, our signal arrives at a set of receivers via multiple paths and the "movement" of each arrival up and down the array of receivers can be compared to the dynamics of a moving target. Hence, the theory developed for target tracking is adapted for our purpose of arrival time estimation. The background and concepts of Bayesian filtering that we follow in our work are discussed in Chapter 3, where initial results from the application of Bayesian filtering to our data are also presented.

Our initial results stimulated our interest in further improving our model by exploring arrival time relationships in space in a more structured way than the one described in Chapter 3. Thus, in Chapter 4, we introduce a new model that treats arrival times as targets, the velocities of which are now estimated as well. These velocities correspond to gradients in the receptions of distinct paths and are

estimated at the same time as actual arrival times. The benefit from the new model is that the knowledge of the gradient from a previous receiver is now one additional piece of information that reduces error in the arrival time estimation process. Another important element that is introduced in Chapter 4 is the estimation of amplitudes of arriving paths in addition to their arrival times. Estimates of amplitudes are essential in estimation of attenuation in seafloor sediments.

Chapter 5 extends our work for cases with an unknown number of ray paths arriving at an array of receivers in the ocean. These cases better reflect realistic situations, where it is not feasible to know *a priori* how many paths are within an observation window. This is the problem of model order estimation often handled with information theoretic criteria. We show that we can extend our method appropriately to estimate the varying number of paths, as well as their arrival times and amplitudes. Not only do we obtain an estimate of the model order, but we also calculate posterior PDFs for the number of paths present in our signals. Our results are further improved in Chapter 6 when, in addition to a forward moving Bayesian filter, we implement a backward filter as well, which allows us to improve estimates by now using information from later states into the estimation process at earlier ones. Finally, in Chapter 7, we apply our estimators to synthetic and real data for estimation of source range, source depth, and water column depth, the task that provided the motivation for our work. Conclusions and future work follow in Chapter 8.

CHAPTER 2

REGULARIZED INVERSION

2.1 Introduction

Sound waves traveling in the ocean "encode" information related to the sea environment and propagation geometry. The recovery of this information using acoustic measurements is the main objective of inverse methods in ocean acoustics.

The properties of the seafloor sediments in shallow water environments have a significant impact on acoustic propagation, making the study of these characteristics of utmost importance. Core survey methods are often time consuming and restricted to small areas. Instead, information about ocean properties can be obtained from data acquired in simple ways (travel time, phase, etc.) via inversion. Various inversion methods based on full-field methods and global optimization [1, 24, 25] or linearization [26, 27, 11] have been presented in the ocean acoustics literature. Details of inverse theory can be found in [28, 29, 30, 31, 32].

Linearized inversion [33, 34] via regularization is employed in this chapter for the estimation of geometric parameters (source and receiver location, and ocean bottom depth). These can be later used for the estimation of sound speed in the sediment layer. The method is applied to acoustic data recorded during an experiment in the Haro Strait, south of Vancouver Island. Broadband sound signals, generated by implosion of household light bulbs, propagated in a range-dependent shallow water region and were received at vertical element arrays. There are three such arrays, referred to as the SW, NW, and NE, because of their location. Although these were vertical line arrays (VLAs), there were also horizontal displacements between phones because of tilt. All arrays consisted of 16 phones (four of those were not operational at the NW array).

The transmitted sound signals arrived at the VLAs via different paths (for example, direct, surface reflection (SR), bottom reflection (BR), bottom surface reflected (BSR), surface bottom reflected (SBR) and other ray paths that interacted with the seabed sediments). Because of the frequency content of the source signals (between 100 and 800 Hz), the distinct arrivals in the received acoustic data are well resolved, as shown in Figure 2.1, which illustrates a set of receptions at the 16 receiving phones of the SW VLA.

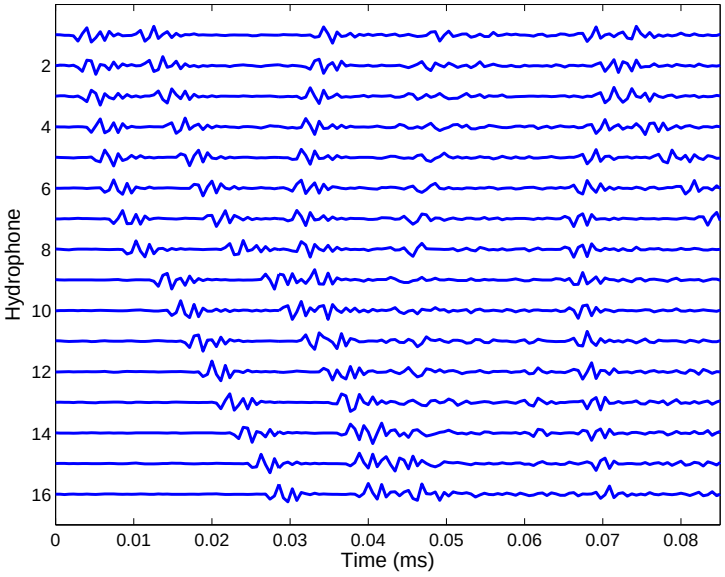

Figure 2.1 Received time-series at the SW array.

The details of the experiment are available in [35, 36].

The problem is formulated by assuming a discrete model $\mathbf{q}$ of unknown parameters and generating replica arrival times using an assumed geometry and environment. The GS-MAP estimation method mentioned in the previous section is employed for the extraction of direct, SR, and BR arrival times from the recorded time-series. An effort is then made to equate the two sets of arrival times, replicas and estimates of measurements, yielding a simple inversion problem. Sections 2.2 and 2.3 discuss linearized inversion using regularization.

In [11], Michalopoulou and Ma employed linearization to estimate the geometric

and environmental parameters assuming a flat bottom. Our aim in this chapter is to improve on these results by including slope in the ocean floor model. Section 2.4 presents the inversion approach applied to Haro Strait data with the consideration of slope. Section 2.5 discusses the inversion results using data from two sources lying on the same 'line of sight.'

2.2 Linearization and Inversion

Inversion via linearization compares measured arrival times of various paths to theoretically and numerically predicted arrival times (replicas), generated using prior knowledge on geometry and environment. The arrival times depend on geometry and environmental parameters of the underwater medium under study, such as source range r, source depth z_s, ocean depth D, receiver depths z_r, source instant t_s, and sound speed c. For the Haro Strait experiment, the sound speed in the water column is assumed to be known and constant with depth, that is, an iso-velocity sound profile is considered with $c = 1482.5\ m/s$. Other parameters like density and sediment attenuation do not affect arrival times and are, hence, ignored.

Arrival times $\mathbf{t}$ are here expressed as:

$$\mathbf{t} = \mathbf{t}(r, z_s, z_r, D) + t_s. \tag{2.1}$$

In our study of Haro Strait data, the measured data $\mathbf{t}$ consist of three arrival times: direct, SR, and BR received at a tilted (and distorted) vertical array of L hydrophones. The success of the method relies on the correct identification and estimation of the different paths carrying sound from the source to the array. We implement the GS-MAP approach for computation of joint PDFs of the unknown parameters. This approach will be addressed later in detail in Chapter 3.

Let vector $\mathbf{q}$ contain the set of parameters to be estimated:

$$\mathbf{q} = [r_1, r_2, \ldots, r_L, z_s, z_{r1}, z_{r2}, \ldots, z_{rL}, D, \phi, t_s] \tag{2.2}$$

where,

- r_i, $i = 1, ..., L$, horizontal ranges of source from L receivers
- z_s, source depth
- z_{ri}, $i = 1, ..., L$, receiver depths
- D, ocean depth
- ϕ, slope of ocean bottom
- t_s, source instant.

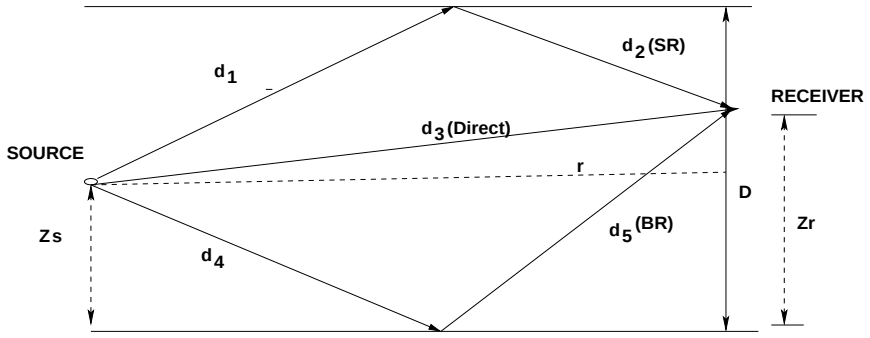

Figure 2.2 Geometry of the environment (the ocean bottom is assumed to be flat).

The geometry of the environment (including the source and VLA positions) is used to relate times to model parameters. As an example, we focus here on the SR path. As shown in Figure 2.2, let $D_{SR} = d_1 + d_2$ be the total distance traveled by the SR ray. The time needed for the ray to travel from source to receiver is:

$$t_{SR} \;=\; t_s + \frac{D_{SR}}{c} \tag{2.3}$$

$$= \quad t_s + \frac{\sqrt{r^2 + (z_s + z_r)^2}}{c}. \tag{2.4}$$

Equation (2.3) above can be generalized as:

$$\mathbf{t} = \mathbf{f}(\mathbf{q}), \tag{2.5}$$

where $\mathbf{f}$ is the forward model relating data and unknown parameters. The relationships between time and $\mathbf{q}$ are mildly non-linear but can be linearized using Newton's method. Linearization leads to:

$$\mathbf{t} = \mathbf{t_0} + \mathbf{J}(\mathbf{q} - \mathbf{q_0}) \tag{2.6}$$

$$\mathbf{Jq} = \mathbf{t} - \mathbf{f}(\mathbf{q_0}) + \mathbf{Jq_0} = \mathbf{d}, \tag{2.7}$$

where $\mathbf{J}$ is the Jacobian matrix containing time derivatives with respect to model parameters, and $\mathbf{t_0}, \mathbf{q_0}$ are vectors formed from initial conditions.

The resulting system can be solved iteratively with least squares. The least squares solution is given by:

$$\hat{\mathbf{q}} = (\mathbf{J^T J})^{-1} \mathbf{J^T t}. \tag{2.8}$$

This expression is based on the assumption that measurement errors are zero-mean Gaussian with the same variance and no correlation. Under these assumptions,

$\hat{\mathbf{q}}$ is the best linear unbiased estimator of $\mathbf{q}$. If, however, the measurements have different uncertainties, a weighted sum of squared residuals is minimized where each weight is equal to the reciprocal of the variance of the measurement. Correlation can also be included in a straightforward manner. Equation 2.7 can then be solved by minimizing the χ^2 misfit:

$$\chi^2 \quad = \quad \|\mathbf{G}(\mathbf{Jq} - \mathbf{d})\|^2 \tag{2.9}$$

with respect to the model $\mathbf{q}$, where $\mathbf{G}$=diag$[1/\nu_1, \ldots, 1/\nu_L]$ is a matrix that weighs the data according to their uncertainties. If the observation errors are uncorrelated, the weight matrix $\mathbf{G}$ is diagonal and equal to the inverse of the covariance matrix of the observations. We assume the observation errors to be uncorrelated and hence the weight matrix $\mathbf{G}$ is diagonal. The solution obtained is:

$$\hat{\mathbf{q}} = (\mathbf{J^T G^T G J})^{-1}(\mathbf{J^T G^T G d}). \tag{2.10}$$

2.3 Regularization

The matrix to be inverted in Equation 2.10 is required to be non-singular and well conditioned; the latter is not typically the case. To remedy this complication, regularization is employed to provide a stable solution to the inverse problem. As suggested in [27, 37, 38], the problem can be regularized by including prior knowledge on the unknown parameters, producing a new objective function:

$$g(q) = \|\mathbf{G}(\mathbf{Jq} - \mathbf{d})\|^2 + \alpha^2\|\mathbf{H}(\mathbf{q} - \mathbf{q_0})\|^2, \tag{2.11}$$

where $\mathbf{H}$ is the regularization matrix that penalizes estimates $\mathbf{q}$ which are far away from the prior information vector $\mathbf{q_0}$. If prior information on model parameters is available, then $\mathbf{H}$ can be chosen to be:

$$\mathbf{H} = diag[1/\xi_1, \ldots, 1/\xi_L], \tag{2.12}$$

where ξ_j represents the uncertainty on the j^{th} parameter. If no information is present for a certain parameter, then the corresponding entry in $\mathbf{H}$ is equal to 0. The regularized solution can be obtained as follows:

$$\hat{\mathbf{q}} = (\mathbf{J^T G^T G J} + \alpha^2 \mathbf{H^T H})^{-1} (\mathbf{J^T G^T G t} + \alpha^2 \mathbf{H^T H q_p}). \tag{2.13}$$

Parameter α is the trade-off value between regularization error and model-data fit. Its value can be selected using an L-curve analysis [30, 11]. The method gets its name from the fact that, when term $\|\mathbf{H}(\mathbf{q} - \mathbf{q_p})\|^2$ is plotted against term $\|\mathbf{G}(\mathbf{Jq} - \mathbf{d})\|$ for various values of α, the resulting graph is an L-shaped curve. An often proposed "optimal" value for α is the one that provides a solution to the right of the corner of the L-curve [39].

2.4 Geometric Relations Between Unknown Parameters for an Ocean Bottom with a Slope

This section aims at improving results obtained for flat bottom geometry in [11, 40] by considering a more accurate description of the true propagation environment. A slope in the ocean bottom is introduced (Figure 2.3) and, accordingly, relations

between the unknown parameters (geometric and environmental) and the measured data $\mathbf{t}$ are described. This problem was also discussed in [41], where parameters were estimated through an exhaustive minimization of differences between measured and replica arrivals. Instead of an exhaustive search, we use the method of linearization and regularization to determine values for the unknown parameters. The vector $\mathbf{q}$ of unknown parameters to be estimated is given by Equation 2.2.

We introduce a new vector $\tilde{\mathbf{q}}$:

$$\tilde{\mathbf{q}} = [r_1^{'}, r_2^{'}, \ldots, r_L^{'}, z_s^{'}, z_{r1}^{'}, z_{r2}^{'}, \ldots, z_{rL}^{'}, D, \phi, t_s], \tag{2.14}$$

where parameters $r_i^{'}$,$z_{ri}^{'}$ and $z_s^{'}$ are introduced for computational purposes and are shown in Figure 2.3.

- D, ocean depth at source location
- $z_{ri}^{'}$, distance between receiver and bottom with slope
- $z_s^{'}$, distance between source and bottom with slope
- $r_i^{'}$, horizontal range from source to the phone with respect to the bottom
- ϕ, angle of inclination of the bottom from the horizontal
- t_s, initial time instant

Using the simple geometry shown in Figure 2.3, we can write the forward model relating data and unknown/uncertain parameters as:

$$t_{di} = t_s + \frac{\sqrt{r_i^2 + (z_s - z_{ri})^2}}{c} \tag{2.15}$$

$$t_{si} = t_s + \frac{\sqrt{r_i^2 + (z_s + z_{ri})^2}}{c} \tag{2.16}$$

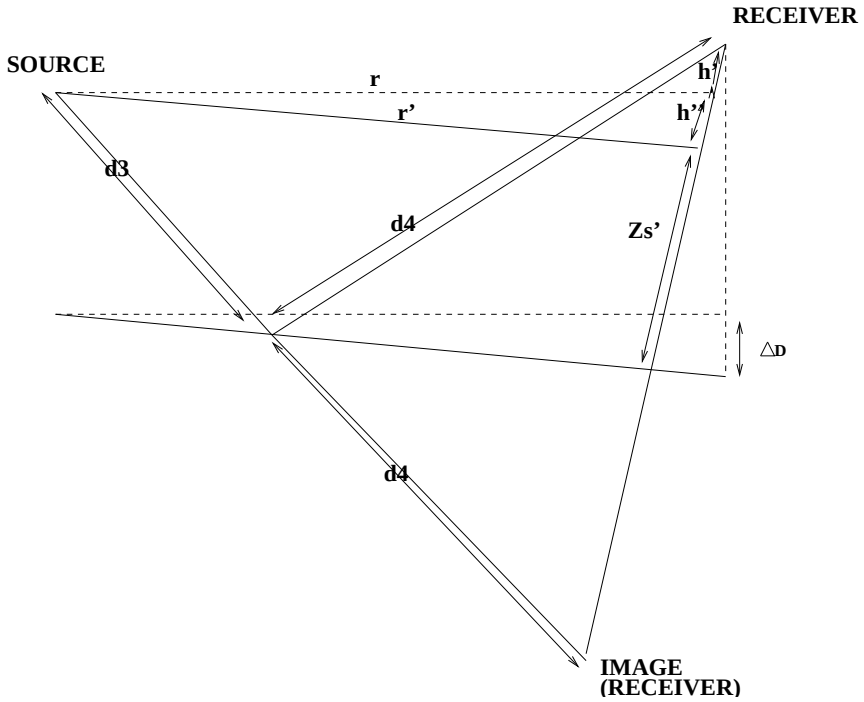

Figure 2.3 Haro Strait geometry with a sloping bottom.

$$t_{bi} = t_s + \frac{\sqrt{r_i^{'2} + (z_s^{'} + z_{ri}^{'})^2}}{c}. \tag{2.17}$$

Also:

$$r_i^{'} = \cos\phi[r_i - (z_s - z_{ri})\tan\phi] \tag{2.18}$$

$$z_{ri}^{'} = \cos\phi[D - z_{ri} + r_i\tan\phi] \tag{2.19}$$

$$z_s^{'} = z_{ri}^{'} - h' - h^{''}, \tag{2.20}$$

where,

$$h' = (z_s - z_{ri})\sec\phi \tag{2.21}$$

$$h^{''} = \sin\phi(r_i - (z_s - z_{ri})\tan\phi). \tag{2.22}$$

Therefore,

$$z_s^{'} + z_{ri}^{'} = 2\cos\phi(D - z_{ri}) + r_i\sin\phi + (z_s - z_{ri})(\tan\phi\sin\phi - \sec\phi). \tag{2.23}$$

Substituting Equations 2.18 and 2.23 into Equation 2.17, we obtain an equation for the first bottom reflected path arrival time.

The relations as described by the above equations can be linearized in a straightforward manner, and the arrival time derivatives with respect to the unknown parameters constitute the entries of the Jacobian matrix **J**:

$$\mathbf{J} = \begin{pmatrix} \frac{\partial t_{d1}}{\partial r_1} \cdots \frac{\partial t_{d1}}{\partial r_L} & \frac{\partial t_{d1}}{\partial z_s} & \frac{\partial t_{d1}}{\partial z_{r1}} \cdots \frac{\partial t_{d1}}{\partial z_{rL}} & \frac{\partial t_{d1}}{\partial D} & \frac{\partial t_{d1}}{\partial t_s} \\ \vdots & & & & \\ \frac{\partial t_{dL}}{\partial r_1} \cdots \frac{\partial t_{dL}}{\partial r_L} & \frac{\partial t_{dL}}{\partial z_s} & \frac{\partial t_{dL}}{\partial z_{r1}} \cdots \frac{\partial t_{dL}}{\partial z_{rL}} & \frac{\partial t_{dL}}{\partial D} & \frac{\partial t_{dL}}{\partial t_s} \\ \\ \frac{\partial t_{s1}}{\partial r_1} \cdots \frac{\partial t_{s1}}{\partial r_L} & \frac{\partial t_{s1}}{\partial z_s} & \frac{\partial t_{s1}}{\partial z_{r1}} \cdots \frac{\partial t_{s1}}{\partial z_{rL}} & \frac{\partial t_{s1}}{\partial D} & \frac{\partial t_{s1}}{\partial t_s} \\ \vdots & & & & \\ \frac{\partial t_{sL}}{\partial r_1} \cdots \frac{\partial t_{sL}}{\partial r_L} & \frac{\partial t_{sL}}{\partial z_s} & \frac{\partial t_{sL}}{\partial z_{r1}} \cdots \frac{\partial t_{sL}}{\partial z_{rL}} & \frac{\partial t_{sL}}{\partial D} & \frac{\partial t_{sL}}{\partial t_s} \\ \vdots & & & & \end{pmatrix}. \tag{2.24}$$

where some of the entries are zero because the direct and SR arrivals do not depend on the depth of the ocean. That is,

$$\frac{\partial t_{di}}{\partial D} = 0 \tag{2.25}$$

$$\frac{\partial t_{si}}{\partial D} = 0 \tag{2.26}$$

$$\begin{aligned}\frac{\partial t_{bi}}{\partial r_i} &= [\cos\phi(r_i - (z_s - z_{ri})\tan\phi)] + \\ &[(2\cos\phi(D - z_{ri}) + r_i\sin\phi + (z_s - z_{ri})(\tan\phi\sin\phi - \sec\phi))\sin\phi] \\ &(-c([(\cos\phi(r_i - (z_s - z_{ri})\tan\phi))^2 + \\ &(2\cos\phi(D - z_{ri}) + r_i\sin\phi + (z_s - z_{ri})(\tan\phi\sin\phi - \sec\phi))^2])^{-1/2}\end{aligned} \tag{2.27}$$

$$\begin{aligned}\frac{\partial t_{bi}}{\partial D} &= [(2\cos\phi(D - z_{ri}) + r_i\sin\phi + (z_s - z_{ri})(\tan\phi\sin\phi - \sec\phi))2\cos\phi] \\ &(-1/c)([(\cos\phi(r_i - (z_s - z_{ri})\tan\phi))^2 + \\ &(2\cos\phi(D - z_{ri}) + r_i\sin\phi + (z_s - z_{ri})(\tan\phi\sin\phi - \sec\phi))^2])^{-1/2}\end{aligned} \tag{2.28}$$

2.4.1 Case NW24

The regularization method discussed in Section 2.3 was applied to Haro Strait data for signal NW24 (implying that shot 24 was considered as the source and the signal was received at the NW VLA). Prior information was available on receiver depths z_{ri}, $i = 1, \ldots, 12$, and ocean depth D, which was taken into account. Uncertainty on receiver and water depths was selected as 5 and 20 m, respectively.

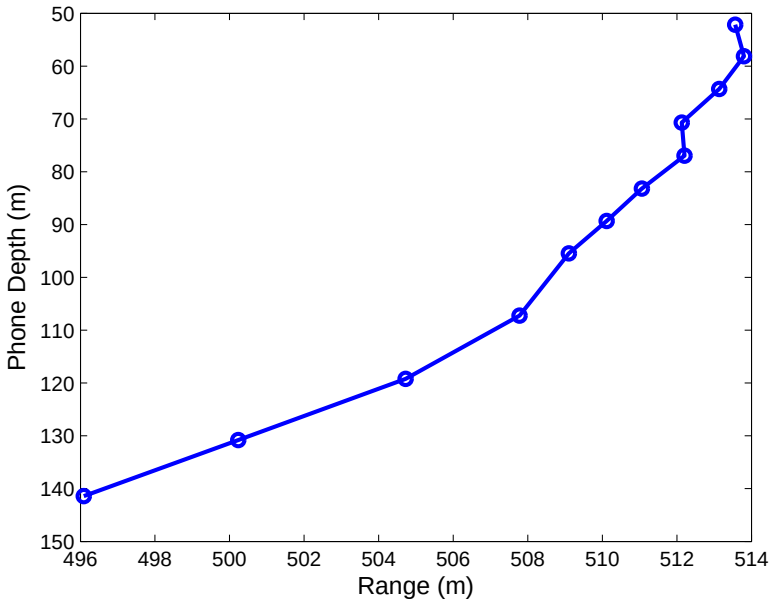

Figure 2.4 Source-receiver ranges and phone depths for case NW24, when slope is also included in the unknown parameters.

Estimates for unknown parameters values were computed via inversion of the NW24 data. The results are shown in Figure 2.4. The estimates for phone depths are plotted against the horizontal distances from the source and demonstrate a tilt in the array.

Table 2.1 shows reference values for source range, source depth, and ocean depth for NW24 and estimates obtained by a obtained for a flat and sloping ocean bottom. For comparison purposes, the same uncertainties were used in both the cases.

2.5 Inversion with two Sources

In this section, we use arrival time data from two sources lying in the same 'line of sight' for better estimation of the unknown parameters, namely, range, source depth and ocean depth. Let the unknown parameter vector be:

Table 2.1 Comparison of Estimates Obtained Using a Flat Bottom Model vs. a Model of an Ocean Bottom with a Slope for NW24

Parameter	Estimate(flat)	Estimate(slope)	Reference
$r_1(m)$	509.0	513.5	512.9
$z_s(m)$	60.7	61.5	70
$D(m)$	201.7	200	200

$$\mathbf{q} = [r_1, r_2, \ldots, r_L, z_s, z_{r1}, z_{r2}, \ldots, z_{rL}, D, \phi, t_s], \tag{2.29}$$

where all the parameters represent the same quantities as before except for D which is now the ocean depth at the first receiver instead of the ocean depth at the source location. The depths at the remaining $k-1$ receivers and the source are related to D as follows:

$$D_i = D + (r_i - r_1)\tan\phi \tag{2.30}$$

$$D_0 = D - r_1 \tan\phi \tag{2.31}$$

where D_0 is the ocean depth at the source; since the two sources fall in the same line of sight, the angle (slope) is the same. Equations 2.15 and 2.16 remain the same. Equation 2.17 changes to:

$$t_{bi} = t_s + \frac{\sqrt{(N_1)^2 + (N_2)^2}}{c} \tag{2.32}$$

where,

$$\begin{aligned} N_1 &= r_i^{'} \\ &= (\cos\phi(r_i - (z_s - z_{ri})\tan\phi) \end{aligned} \tag{2.33}$$

$$\begin{aligned} N_2 &= z_{snew} + z_{rnew} \end{aligned} \tag{2.34}$$

where,

$$z_{rnew} = (D - z_{ri})\cos\phi + (r_i - r_1)\sin\phi + r_i\sin\phi \tag{2.35}$$

$$z_{snew} = z_{rnew} - h^{'} - h^{''} \tag{2.36}$$

Quantities $h^{'}$ and $h^{''}$ are the same as in Equations (2.21-2.22). Equation (2.35) has been obtained by substituting Equation (2.30) into Equation (2.19).
Thus,

$$N_2 = 2z_{rnew} - h^{'} - h^{''} \tag{2.37}$$

$$\begin{aligned} N_2 &= 2(D - z_{ri})\cos\phi + 2(r_i - r_1)\sin\phi + r_i\sin\phi + \\ &\quad (z_s - z_{ri})(\tan\phi\sin\phi - \sec\phi) \end{aligned} \tag{2.38}$$

With these new equations describing the BR arrival time, the entries related to derivatives of bottom reflected arrival time with respect to the unknown parameters in the Jacobian matrix **J** will change. For instance, the derivative of the BR arrival

time with respect to D becomes:

$$\frac{\partial t_{bi}}{\partial D} = \frac{-2(N_2)\cos\phi}{c\sqrt{N_2}} \tag{2.39}$$

2.5.1 Results: Cases SW29-SW32

Figure 2.5 illustrates the inversion results when data from two sources are employed. The plot illustrates the structure of the array, the depths of the hydrophones, and the positions of the two sources. A tilt in the SW array can be noticed from the shallowest receiver, which is at a depth of approximately 45 m, to the deepest receiver, which is at an approximate depth of 138 m. Source 29 is deployed in an environment that is deeper than that of source 32. The phone array is positioned at an even deeper site in comparison to that of both sources 29 and 32. This environmental description matches prior bathymetry knowledge on the site of the experiment.

Inversion results using data from two sources with a sloping ocean bottom are compared to inversion results obtained using data from one source with a flat ocean bottom in Table (2.2). The results presented in the table using data from two sources and considering a sloping bottom are more accurate in terms of proximity to benchmark values than the results calculated via simple inversion under a flat bathymetry assumption.

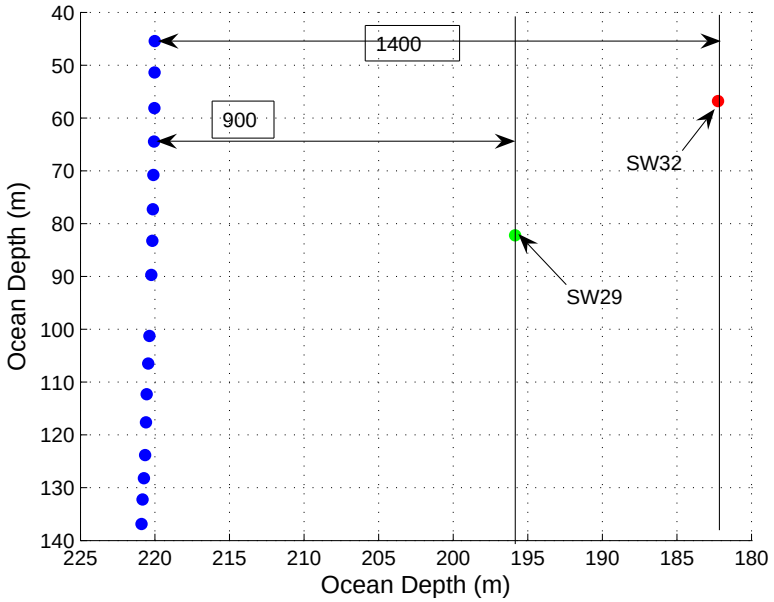

Figure 2.5 Array and source positions for shots 29 and 32 with respect to the SW array.

Table 2.2 Comparison of Estimates for SW29 Obtained Using a Flat Bottom vs. Using Data from Two Sources for a Sloping Ocean Bottom

Parameter	Estimate (flat)	Estimate (2 sources)	Reference
$r_1(m)$	865.8	900.0	894.7
$z_s(m)$	77.0	81.0	70.0
$D(m)$	202.0	195.0	190.0

CHAPTER 3

BAYESIAN FILTERING: A SIMPLE MODEL

3.1 Introduction

In this chapter, the focus is on the estimation of multipath arrival times of a known deterministic signal at a set of L spatially separated hydrophones. Our aim is to estimate both arrival times and amplitudes of paths arriving at L receivers via various paths such as direct, surface reflection, and bottom reflection. To obtain these estimates, we first calculate the joint PDF for amplitudes ($\tilde{a_k} = [a_1, a_2, ..., a_P]$, $k = 1, \ldots, L$, P being the number of arrivals) and arrival times ($\tilde{X_k}$), where each $\tilde{X_k}$ consists of different paths (such as the ones mentioned above). Thus, $\tilde{X_k}$ is a vector: $\tilde{X_k} = [X_1, X_2, ..., X_P]$. The PDF we want to compute is
$p(\tilde{a_1}, \tilde{a_2}, \tilde{a_3}..., \tilde{a_L}, \tilde{X_1}, ..., \tilde{X_L}|Y_1, ..., Y_L)$, where Y_k, $k = 1, \ldots, L$, is the received signal at the k^{th} receiver. Signal Y_k can be written as:

$$Y_k(t) = \sum_{p=1}^{P} a_{kp} s(t - X_{kp}) + n_k(t), \tag{3.1}$$

where $t = 1, \ldots, N_s$ (N_s is the duration of Y_k) [19, 42, 43, 44]. Quantity a_{kp} is the amplitude of the p^{th} path at the k^{th} receiver and n_k is additive white Gaussian noise. Figure 3.1 shows five time-series Y_k ($k = 1, 2, 3, 4, 5$) at five phones of a VLA, consisting of $P = 2$ arrivals. Estimates of arrival times of paths in Figure (3.1) and their corresponding amplitudes can be obtained by calculating the mean or mode of their joint PDF. The latter provides MAP estimates.

Maximizing the joint PDF $p(\tilde{a_k}, \tilde{X_k} \mid Y_k)$ of amplitudes and arrivals is an optimal way for estimating arrival times and amplitudes at a particular receiver [45],

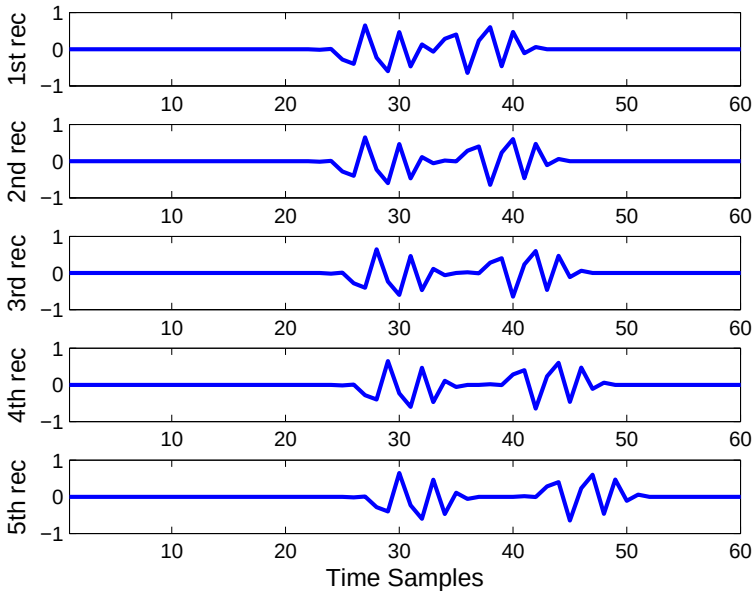

Figure 3.1 Time-series for the first five receivers.

but it can get computationally expensive as the number of paths increases. An efficient method developed in [19] is the implementation of a MAP approach for amplitude and arrival time estimation using Gibbs Sampling (GS-MAP). The Gibbs Sampler was used for the computation of full joint PDFs of amplitudes and arrival times at every receiver. The method is briefly described below.

Assuming a uniform prior on amplitudes and arrival times as:

$$p(a_i) = 1 \quad -\infty < a_i < \infty, \quad i = 1, ..., P \tag{3.2}$$

$$p(X_i) = \frac{1}{N_s} \quad 1 \leq X_i \leq N_s, \quad i = 1, ..., P, \tag{3.3}$$

the joint posterior PDF at receiver k has the form:

$$p(X_1, X_2, ..., X_P, a_1, a_2, ..., a_P | Y_k) = C \frac{1}{N_s^P} \frac{1}{\sqrt{2\pi\sigma^2}^{N_s}} \exp(-\frac{1}{2\sigma^2} \sum_{t=1}^{N_s} (Y_k(t) - \sum_{p=1}^{P} a_p s(t - X_p))^2) \tag{3.4}$$

where C is a normalizing constant.

Gibbs Sampling is an iterative Monte Carlo (MC) process used to sample from a joint distribution which is not known explicitly, when the conditional distribution of each variable conditional on the current values of other variables is known [46, 47, 20, 48, 49].

The joint PDF of arrival times and amplitudes as shown by Equation (3.4) is obtained by computing the marginal distribution of each unknown parameter conditional on other parameters; for example, the conditional posterior distribution of X_1 for known $X_2, ..., X_P$ and a_p, $p = 1, 2, ..., P$, is:

$$p(X_1 \mid X_2, ..., X_P, a_1, a_2, ..., a_P, Y_k) = G \exp(-\frac{1}{2\sigma^2} \sum_{t=1}^{Ns} (Y_k(t) - \sum_{p=1}^{P} a_p s(t - X_p))^2). \quad (3.5)$$

The conditional distributions serve as building blocks for the estimation of the joint PDF of arrival times and amplitudes. In general, if Y is our data and $\Theta = [\theta_1, \theta_2, ..., \theta_D]$ is a vector of parameters of interest with selected initial values $\Theta^0 = [\theta_1^0, \theta_2^0, ..., \theta_D^0]$, then the following steps are run iteratively:

for $i = 1 : T$

- sample θ_1^{i+1} from $p(\theta_1 | \theta_2^i, ..., \theta_D^i, Y)$
- sample θ_2^{i+1} from $p(\theta_2 | \theta_1^{i+1}, \theta_3^i ..., \theta_D^i, Y)$

  $\vdots$

end

The sequence of vectors $\Theta^0, ..., \Theta^T$ converges to the true PDF for large T [46, 47, 48].

In case of multipath arrivals, it is difficult to associate a particular arrival

to its respective path with GS-MAP. This is one of the drawbacks of GS-MAP that we wish to remedy in our study so that arrival estimates, can be used to enhance inversion. This will facilitate the better understanding of ocean environments.

Another disadvantage of GS-MAP and arrival time estimation methods is that they estimate $\tilde{a_1}, ..., \tilde{a_L}, \tilde{X_1}, ..., \tilde{X_L}$ at every receiver but fail to use information available from neighboring phones. Information from previous or next receivers can be crucial and can provide useful insights in arrival times of distinct paths. Thus, we propose to identify and utilize relations between arrivals from one receiver to another. This approach can be expressed via Bayes rule as follows:

$$\begin{aligned} p(\tilde{a_1}, ..., \tilde{a_L}, \tilde{X_1}, ..., \tilde{X_L}|Y_1, ..., Y_L) &= p(\tilde{a_L}, \tilde{X_L}|\tilde{a_{L-1}}, \tilde{X_{L-1}}, Y_L) \\ & \quad p(\tilde{a_{L-1}}, \tilde{X_{L-1}}|\tilde{a_{L-2}}, \tilde{X_{L-2}}, Y_{L-1}) \\ & \ldots \quad p(\tilde{a_2}, \tilde{X_2}|\tilde{a_1}, \tilde{X_1}, Y_2)p(\tilde{a_1}, \tilde{X_1}|Y_1). \end{aligned} \tag{3.6}$$

Hence, if a prior $p(\tilde{a_1}, \tilde{X_1}|Y_1)$ at the first receiver is selected, the joint PDF of amplitudes and arrival times can be estimated for the following receivers using a Bayesian filter.

3.2 State-Space Model

The idea of Bayesian filtering has been used extensively for target tracking, that is, estimating a target's position (flight corridors for commercial planes, road network for civil surveillance, etc) from time t to time $t + 1$.

The signal arriving at an array of spatially separated receivers can be compared to a source moving in time and the idea of target tracking (tracking a target's position, velocity, or acceleration in time) can be used in our study to track arrival times in

space. We view every path as a target and track it in space as if we were tracking a target in time. Thus, the theory developed for conventional target tracking can be used to track the various paths in space, enabling us to estimate arrival times and amplitudes from one receiver to another in a particular time frame.

We adopt a state-space approach [50, 51, 52, 53, 54, 55] to model the dynamics of the system. That is, every possible position (represented by a time sample) and its corresponding signal strength (amplitude) are represented as a state and the probability of moving from one state to another depends only on the previous state. This property is known as the Markov property. In general, the state vector contains all relevant information that might be required to describe the system; for example, position and velocity (and, later, signal amplitudes) of a 'target' in time or space. Here, we consider L hydrophones placed in an ocean environment. Arrival times evolve from one receiver to the next. Hence, our problem narrows down to estimation of arrival times in space within a particular time frame.

In order to analyze the dynamics of such a system, two models are required: (a) a model to describe the transition of states from receiver k to $k+1$, and (b) a model to relate the noisy measurements at receiver $k+1$ to the state.

Let X_k be the state vector at state k. Its expected evolution in space can be expressed via the prediction equation (reflecting the transition model):

$$X_k = F_k(X_{k-1}, w_k) \tag{3.7}$$

The actual measurements and state are related by the update-observation equation:

$$Y_k = H_k(X_k, n_k) \tag{3.8}$$

Here, (w_k, n_k) represent independent and spatially and temporally uncorrelated noise, that is, the covariance matrices of w_k and n_k is a diagonal matrix. Functions F_k, H_k are, in general, nonlinear, and X_k, Y_k are multi-dimensional vectors. The goal is to estimate X_k based on the set of available measurements Y_k. For that, we will first calculate PDF $p(X_k \mid Y_k)$.

Assuming that PDF $p(X_{k-1} \mid Y_{k-1})$ is known at state $k-1$, the PDF of arrival times for the current step k can be computed using the following recursion equation [42]:

$$p(X_k \mid Y_{k-1}) = \int p(X_k \mid X_{k-1}) p(X_{k-1} \mid Y_{k-1}) dX_{k-1} \tag{3.9}$$

(Chapman-Kolmogorov Equation)

$$p(X_k \mid Y_k) \propto p(Y_k \mid X_k) p(X_k \mid Y_{k-1}). \tag{3.10}$$

(Bayes rule)

In general, $p(Y_k \mid X_k)$ denotes the density of Y_k given parameter values X_k. For a particular value of $X_k = x_k$, after data Y_k have been observed, $p(Y_k \mid X_k)$ becomes a likelihood function for X_k. Any reference to $p(Y_k \mid X_k)$ henceforth, will represent the likelihood function rather than the PDF of Y_k.

Using the PDF described in Equation (3.10), we can obtain parameter estimates such as expectation [56]:

$$\hat{X}_k = E(X_k \mid Y_k) = \int X_k p(X_k \mid Y_k) dX_k \tag{3.11}$$

or a MAP estimate as,

$$\tilde{\hat{X}}_k = \arg \ \ max \ \ p(X_k \mid Y_k). \tag{3.12}$$

Because the PDF is not necessarily Gaussian or even unimodal, the mode is the estimator we will be computing, since the mean may be misleading.

The situation would have been simple had all the PDFs been available in closed forms and easy to compute, which is usually not the case in practical situations. If the PDF at every step is Gaussian and functions H_k and F_k are linear, the Kalman Filter (KF) [50, 57, 58, 56, 59, 51] is the optimal Bayesian filter for estimating unknown parameters such as ours. Under these circumstances, Equations (3.7) and (3.8) can be written in the following form:

$$X_k = F_{k-1}X_{k-1} + w_{k-1} \tag{3.13}$$

$$Y_k = H_kX_k + n_k, \tag{3.14}$$

where w_k and n_k follow Gaussian distributions. From Equation (3.7), we can obtain the state transition probability $\mathrm{p}(X_k \mid X_{k-1})$. Equation (3.8) is employed to obtain the likelihood function $\mathrm{p}(Y_k \mid X_k)$. Thus, the PDF $p(X_k \mid Y_k)$ can be calculated recursively using the prediction and update Equations (3.9) and (3.10).

For nonlinear systems where functions F and H can be linearized using a Taylor expansion, an Extended Kalman Filter (EKF) is often used for parameter estimation [60, 61]. Assuming that nonlinearities in H and F are small, these functions are approximated by the first term in their Taylor series expansion. This filter is sometimes referred to as an analytic approximation because the nonlinear functions are expanded analytically. If the nonlinearity is significant and the functions

and noise components follow complex distributions, EFKs are not applicable. If the PDF p($X_k \mid Y_k$) is moderately non-Gaussian and can be represented by the first two moments, then an Unscented Kalman Filter (UKF) can be employed [62]. Instead of linearizing functions F and H, the UKF approximates the PDF $p(X_k \mid Y_k)$ with a Gaussian distribution. Thus, linearization is obtained in a statistical sense rather than an analytical one. A particle filter (PF), on the other hand, is a Bayesian filter that does not require either the assumption of Gaussian PDFs or linearity and can be employed when the KF and its extensions fail due to the nonlinear structure of the state and measurement equations and the non-Gaussian behavior of measurement errors. PF is a sequential Monte Carlo (SMC) method [63, 64, 65, 66, 67] that uses a set of particles to represent the required PDF [68, 69, 70, 71, 72, 73]. It is an approach that executes the recursive Bayesian filter through MC simulations. Since, in the implementation of a PF, the PDF of the state vector at the present step is used for the prediction of the state vector at the next step, the PF is often referred to as a sequential tracker.

We use the idea of particle filtering and represent the PDF by a set of particles, where every particle is of the form $X_k = [X_1, X_2, ..., X_P]$. Sequential Importance Sampling (SIS) and Sampling Importance Resampling (SIR) are two of the many kinds of particle filters that are most common [74, 55, 56] and will be discussed in brief in the following sections.

3.3 Particle Filtering

This section discusses the implementation of PFs in our problem. Once the transition densities and likelihood function have been obtained, a PF is designed to obtain the PDF of the arrival times-direct and SR in the beginning and more paths later on.

3.3.1 Sequential Importance Sampling Algorithm

SIS is a technique used for implementing recursive Bayesian filtering via Monte Carlo simulations. Let the required posterior PDF be denoted as $p(X_k \mid Y_k)$, where $\{X_k^i, i = 1...N\}$ is a set of support points for the unknown parameters and Y_k are the received data at receiver k [74].

Let $\{w_k^i, i = 1...N\}$ be the associated weights corresponding to the support points. These weights are normalized so that $\sum_i w_k^i = 1$. Then, the posterior PDF of X_k at receiver k can be described as [63]:

$$p(X_k \mid Y_k) \approx \sum_{i=1}^{N} w_k^i \delta(X_k - X_k^i). \tag{3.15}$$

The weights are assigned to states X_k^i through the likelihood function $p(Y_k \mid X_k)$. This will be discussed in more detail later.

The discrete weighted approximate representation is an unbiased estimate of the true posterior PDF and approaches the true PDF as $N \to \infty$ [56].

Typically, it is not easy to obtain a closed form of the posterior density; instead, samples X_k are drawn from a known and simpler density $q(X_k \mid Y_k)$, which is called the importance or proposal density. The importance density is similar to the original density function, that is, they have the same set of support points. Hence, the weights are now defined as:

$$w^i \propto \frac{p(X_k^i \mid Y_k)}{q(X_k^i \mid Y_k)}. \tag{3.16}$$

The weights in Equation (3.16) are obtained from Monte Carlo integration, the details of which can be found in [56].

Assuming that the posterior PDF at state $k-1$ is known, the importance density can be written as:

$$q(X_k) = q(X_k \mid X_{k-1})q(X_{k-1} \mid Y_{k-1}). \tag{3.17}$$

The new set of samples at receiver k, $X_k^i \sim q(X_k^i \mid Y_k)$, can be obtained by augmenting each of the existing samples $X_{k-1}^i \sim q(X_{k-1}^i \mid Y_{k-1})$ with the new state $X_k^i \sim q(X_k^i \mid X_{k-1})$. The weight equation is then:

$$w_k^i \propto \frac{p(Y_k \mid X_k^i)p(X_k^i \mid X_{k-1}^i)p(X_{k-1}^i \mid Y_k)}{q(X_k^i \mid X_{k-1}^i)q(X_{k-1}^i \mid Y_{k-1})} \tag{3.18}$$

$$w_k^i = w_{k-1}^i \frac{p(Y_k \mid X_k^i)p(X_k^i \mid X_{k-1}^i)}{q(X_k^i \mid X_{k-1}^i)}. \tag{3.19}$$

The weights and support points are propagated recursively as each measurement is received sequentially.

One simple variant of the SIS filter can be derived if the importance density $q(X_k \mid X_{k-1}^i)$ is chosen to be the prior density $p(X_k \mid X_{k-1}^i)$.

3.3.2 SIR: Resampling for Degeneracy Reduction

A common problem with such methods is that, after a few iterations, many particles have negligible weights; a large computational effort is required to update even those particles, whose contribution to the approximation of the posterior PDF is almost zero. This is known as 'degeneracy'. Resampling is an effective way to reduce degeneracy [75, 56]. In resampling, the main idea is to concentrate on particles

with large weights while eliminating particles with smaller ones. Resampling involves generating a new set of particles $X_k^{i*}, i = 1...N$ from the existing data set by sampling with replacement such that $Pr(X_k^{i*} = X_k^j) = w_k^j$. The particle set obtained as a result of resampling is an independent and identically distributed (i.i.d) sample from the discrete density 3.15; therefore, the weights are set to $w_k^i = 1/N$ [74, 56].

Various resampling techniques like 'Residual Resampling', 'Stratified Resampling', 'Multinomial Resampling', and 'Systematic Resampling' are analysed in [75, 76, 77] to reduce the variance amongst particles. The way to resample is via the cumulative density function (CDF) of the weights. Once the CDF has been constructed, a random number from a uniform distribution is selected and compared with the cumulative sum of weights while moving up the CDF, starting from its bottom until the value of the random number is less than the value of the CDF at a point j.

$$u_1 \sim U(0, 1/N) \tag{3.20}$$

$$u_j = u_1 + N^{-1}(j-1), j = 1, ..., N. \tag{3.21}$$

Then, a new particle $X^j = X^i$ is chosen, such that $u_j <= c_i$ and $u_j > c_{i-1}$, where c_i is the value of the cdf at i^{th} particle and $w^j = 1/N$. Drawing particles from the CDF in this manner leaves out particles with negligible weights and, at the same time, particles with larger weights are selected more frequently.

Figure 3.2 shows one iteration of the particle filter with resampling.

Combination of the SIS filter with resampling is known as the Sample Importance Resampling Filter (SIR) filter. This implies that the samples need to be drawn from $p(X_k \mid X_{k-1}^i)$ and the weight equation (Equation (3.16)) can now be written as:

$$w_k^i = w_{k-1}^i p(Y_k \mid X_k^i). \tag{3.22}$$

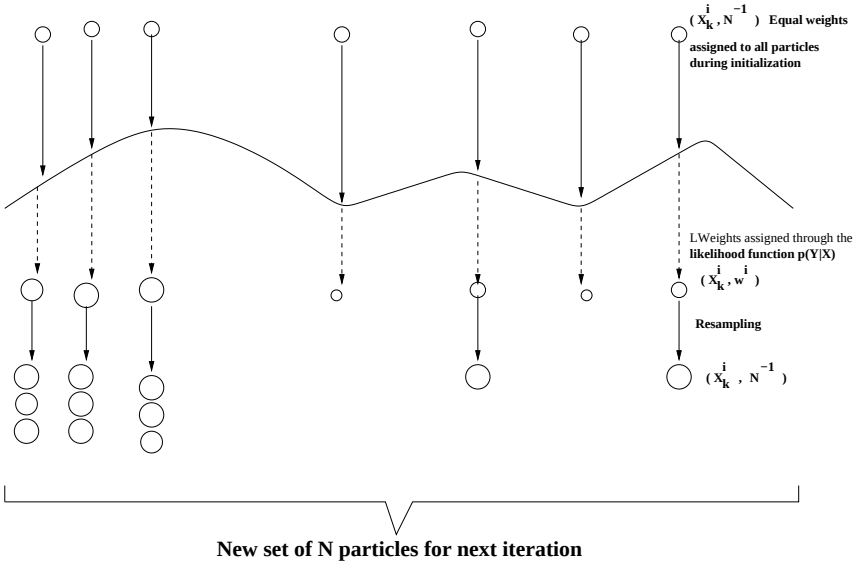

Figure 3.2 Symbolic representation of particle filtering. Particles are denoted by circles, the size of which reflects their corresponding likelihood weights.

Weights are normalized before the resampling stage.

3.3.3 Order of Complexity

The order of complexity of PFs is an important consideration for their implementation. The order is tightly related to the number of particles necessary to attain desired levels of accuracy. Naturally, larger state vectors require more particles. It is expected that the number of particles increases linearly with the number of parameters to be estimated [78]. However, this is not strictly the case, as careful investigation of a particular problem might reveal features (such as linearity between measurements and at least part of the state vector), that can be explored for the reduction in the number of particles. This is known as Rao-Blackwellization and it will be explained in more detail in the following chapter. The order of complexity depends on the method selected for resampling, which, in its turn, is a function of the number on particles.

The order has been found to be $O(N)$ when the resampling procedure described in this paper is adhered to [56].

In addition to the load of resampling, nonlinearities in the state and measurement equation and the level of noise are important factors determining the computation requirements of a particle filter.

3.4 Algorithm Development - Known Number of Paths and Known Amplitudes

To start with, we base our study on just two paths: direct and SR. Hence, the number of paths for initial discussion is two and constant with state (phone). As an example, Figure (3.1) shows the two paths arriving at the first five receiving phones. Our convention is that the first receiver is the one at the shallowest depth. The signal is shown in time samples rather than in true time. True time can be calculated by dividing time samples over the sampling frequency. In our case, both arrivals, direct and SR, arrive close to each other at the first receiver, making it difficult to identify them. This occurrence and its impact will be discussed later.

Amplitudes $a_k = [a_{dk}, a_{sk}]$ of the two arrivals are initially assumed to be known: $a_{dk} = 1$ is the amplitude associated with the direct arrival and $a_{sk} = -1$ is the amplitude associated with the SR arrival. Let X_k=[X_{dk}, X_{sk}] be the unknown state vector at receiver k; X_{dk} represents the direct ray and X_{sk} represents the SR path. Our goal is to estimate X_k given data Y_k and prior states.

To obtain the state transition probability $p(X_k \mid X_{k-1})$ and the likelihood function $p(Y_k \mid X_k)$, we describe the dynamics of the system using the prediction and update equations.

3.4.1 Transition Density

At receiver k, let X_k=[X_{dk}, X_{sk}]. A random walk process is used to model the dynamics of propagation of X_k:

$$X_k = X_{k-1} + w_k, \tag{3.23}$$

where $w_k \sim N(\mathbf{0}, \sigma_k^2\mathbf{I})$, $\mathbf{I}$ being the 2×2 identity matrix. Parameter σ_k is the standard deviation of the direct and SR paths from receiver $(k-1)$ to the receiver k, which is chosen empirically depending on general expectations on the evolution of arrival times. Information on these perturbations can be extracted by simulating sample arrival times at a set of hydrophones representing our array for a set of possible ocean environments and source positions.

The transition density is described by:

$$p(X_k \mid X_{k-1}) \sim N(X_{k-1}, \sigma_k^2). \tag{3.24}$$

3.4.2 The Likelihood Function

Assuming that the signal from a sound source arrives to a set of receiving phones via P paths instead of just a direct eigenray, the measurement model in a nondispersive medium [43] can be written as in Equation 3.1, where $t = 1, \ldots, N_s$ (N_s is the duration of the received signal). The number of paths P is initially considered known. Quantity X_{kp} denotes the arrival time of path p of the k^{th} receiver and a_{kp} is its corresponding amplitude.

The likelihood function using the measurement equation is:

$$p(Y_k \mid X_k) = \exp(-\frac{\sum_{n=1}^{N_s}(Y_k - \sum_{p=1}^{P} a_{kp} s(n - X_{kp}))^2}{2\sigma^2}). \tag{3.25}$$

The likelihood function, instead of being calculated over the entire domain as in the case of ML computations, is now being computed for only few possible time samples (N particles) that lie within a feasible region determined by the transition density function (or a prior density for $k = 1$).

3.5 Implementation

In the tracking problem discussed here, we are interested in tracking the direct and SR arrival evolution across receiving hydrophones. Concatenation of one sample for each of the two paths produces a particle at receiver k. Thus, at the k^{th} receiver, a particle is described by a two-dimensional vector of arrival time samples X_k^i=[X_{dk}^i, X_{sk}^i], $i = 1, \ldots, N$. Element X_{dk}^i represents a sample for the direct arrival and X_{sk}^i represents a sample for SR.

The PF applied here is based on the SIR filter. The filter is initialized by drawing a sample X_{k0}^i, $i = 1, \ldots, N$, from a uniform distribution over the entire range of time samples. Weights for particles w_k^i are computed according to Equation (3.22).

The particles are propagated using the transition density by sampling from a normal distribution $X_k^i \sim N(X_{k-1}^i, \sigma_k^2)$. The computed weights are normalized and resampling is performed, generating a new set of particles from the existing set. Finally, MAP arrival time estimates for the direct and SR arrival at receiver k are computed as the mode of the joint posterior PDF.

3.5.1 Simulation Results - Error Analysis

The above algorithm is validated with simulated data that includes two ray paths: direct and SR. The arrival structure for the two paths is shown in Figure (3.3). Figure (3.4(a)) shows noise-free time-series with two arrivals and Figure (3.4(b)) demonstrates one noisy realization for an SNR of 15 dB.

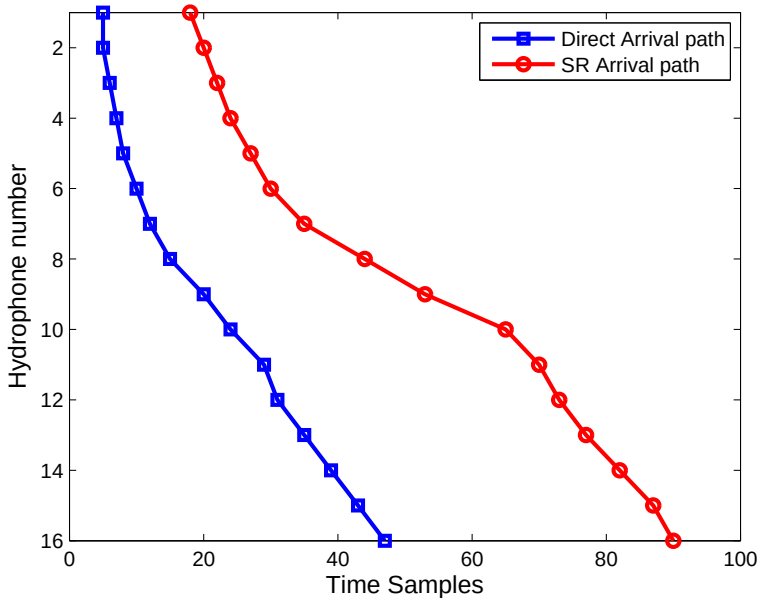

Figure 3.3 Arrival times for the direct and SR paths for a synthetic data set.

Figure (3.5) shows the estimates obtained with the PF and ML estimators for the arrival times of the direct and SR arrivals at a Signal to Noise Ratio (SNR) of 15 dB. The performance of the PF is plotted vs. the number of particles. Here, error is the L_2-norm averaged over $K = 16$ receivers and N_r noisy realizations:

$$error = \sqrt{\frac{\sum_{k=1}^{K} |\mathbf{x}_k - \hat{\mathbf{x}}_k|^2}{K\ N_r}}, \tag{3.26}$$

where $\mathbf{x_k}$ is the vector of true values of the arrival times and $\hat{\mathbf{x}}_\mathbf{k}$ is the vector of the modes of the arrival time PDFs estimated at state k. One-hundred realizations

($N_r = 100$) were run for a Monte Carlo performance evaluation. The error curves were smoothed with a median filter.

The first observation we make is that the PF does not offer an advantage over the ML estimator when the number of particles is small. The reason is that few particles are not adequate for capturing a broad probability density region. As the number of particles increases, the PF outperforms significantly the ML method for the direct path arrival time estimation. However, we note that there exists a substantial difference in the performance of the PF for the direct and SR arrival estimation. Although the PF performance is excellent for the former, the PF error in SR arrival estimation is high, making the ML preferable. This was initially puzzling, since we expected a superior performance in both direct and SR cases. Careful review of the problem and implementation led us to understand that this difference in errors suggests that the sharp changes of the SR arrival times in space (which can be seen in Figure 3.3) are the cause for the significant error. The changes are less steep for the direct path. It appears that the simple PF model is unable to capture the arrival time evolution. In the next chapter, we discuss a new model that improves the results of the particle filter.

3.5.2 Simulation Results - PDF Calculation

Figure (3.6) illustrates estimated PDFs for the direct and SR paths for an SNR of 17 dB using the PF method, which further strengthen our observations from Figure (3.5). At the tenth receiver, the gradient of the PDF for the SR arrival is concentrated in regions far from the true arrival time values. The reason is that the perturbation of the particles at the 9^{th} receiver imposed by the transition density was inadequate for shifting the particles towards the region around the true arrival time at the 10^{th} receiver. Instead, a region away from the true arrival time was populated

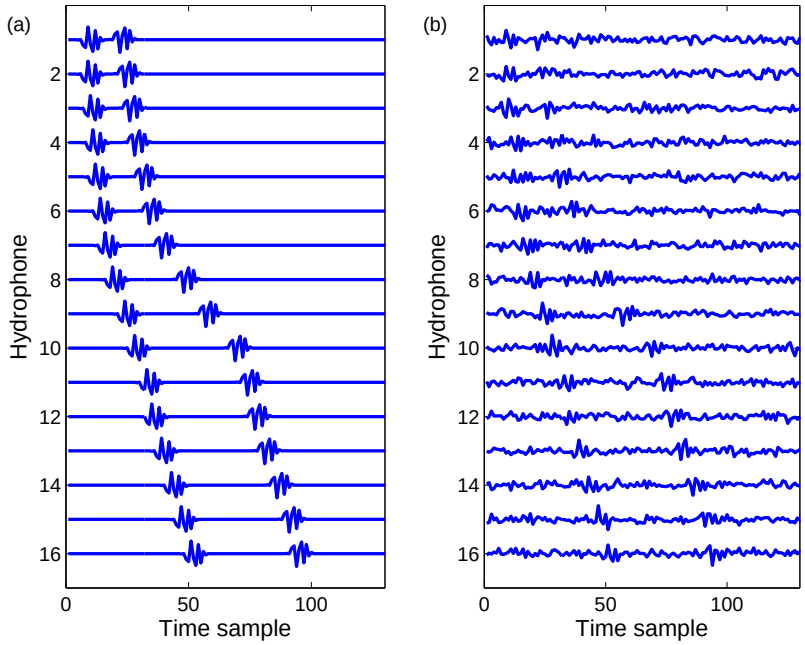

Figure 3.4 Noise-free signal and (b) one noisy realization. The SNR is 15 dB.

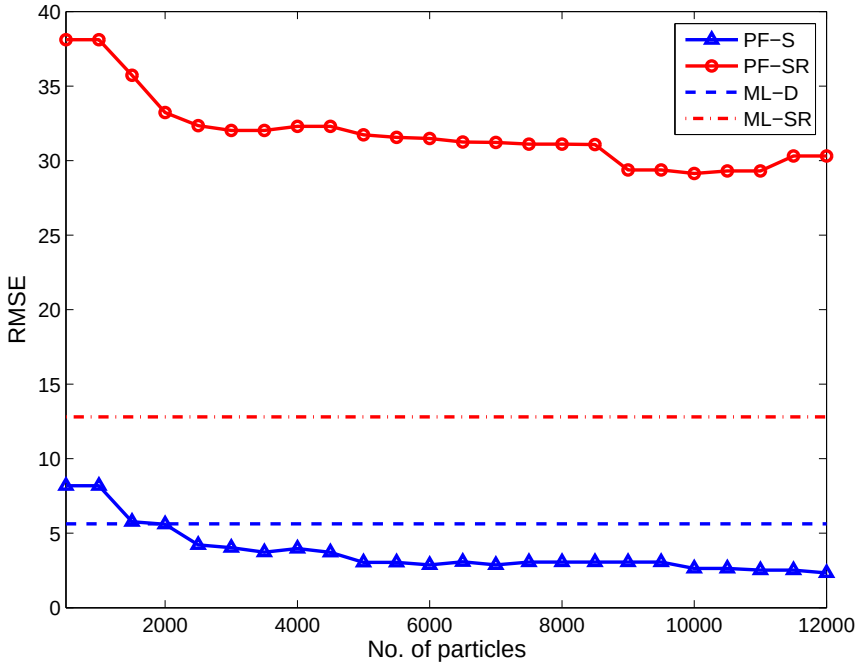

Figure 3.5 Performance of a PF (triangle: direct, circle: SR) and ML (dashed line: direct, dot-dashed line: SR). The SNR is 15 dB.

with particles. In the next chapter, we will discuss how this shortcoming can be remedied.

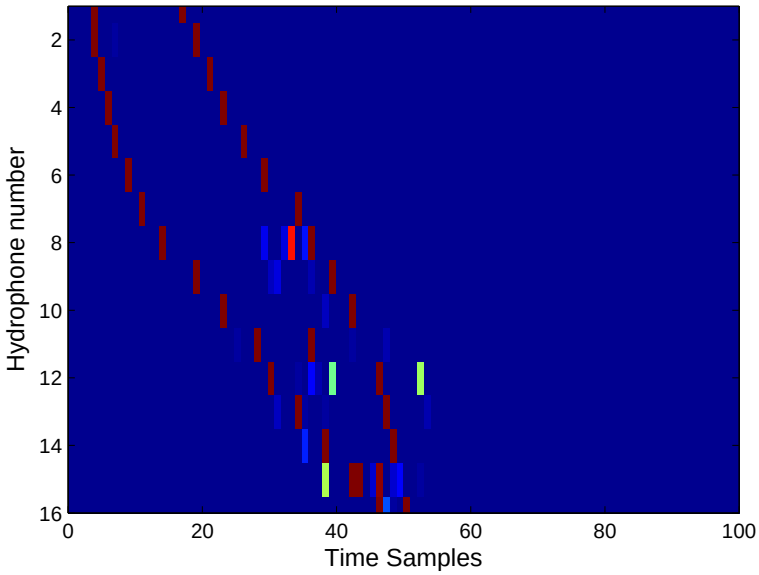

Figure 3.6 Arrival time PDFs for the direct and SR paths.

CHAPTER 4

BAYESIAN FILTERING: DYNAMIC MODEL AND AMPLITUDE ESTIMATION

4.1 Discussion of Practical Implementation Aspects

In the following section, we continue to investigate the reason for results as seen in Chapter 3 and aim to find a solution to density problem. The limitation of the transition density function brought up in the last chapter is more clearly demonstrated in Figure (4.1). Although the transition model suffices for the direct path (top plot), it does not seem to describe adequately the SR arrival: the samples for the surface reflection do not capture the high likelihood region (bottom plot).

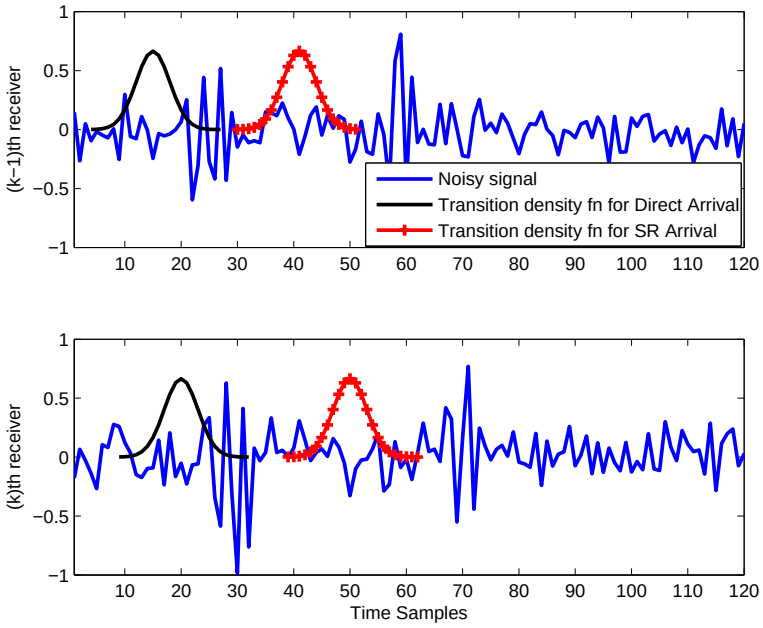

Figure 4.1 A sketch of the transition density function for both direct and SR arrivals.

The arrival path can be compared to the trajectory of a moving target; similarly to a target's position and velocity changing with time, the time at which a

particular path (direct and SR, for example) arrive in our problem change at every receiver. Just like a target's motion model describes the evolution of the target state with respect to time, our motion model describes the evolution of "arrival trajectories" with respect to space. Using kinematic constraints in the model dynamics helps in reducing the bias in the estimates when the actual acceleration is time/position varying [79]. The present transition density function does not take into consideration the velocity/gradient inherent in the arrival time evolution and, hence, fails to prescribe to particles the necessary motion. The transition density function must be updated to include a velocity component for the appropriate particle movement from one receiver to another. A kinematic component is typically incorporated in the transition/prediction equation to integrate velocity into the tracking process. The inclusion of kinematics into the filter is discussed in [80, 81, 82, 56]. Velocity can be dealt with as a constant or as varying with time or space, which is more suitable for our problem. Adapting the approach to our model, we use velocity to represent the gradient of arrival times of a specific path in space.

The simplest model for a target maneuver (model with the kinematic constraint) is the 'white-noise acceleration model' [60], which assumes that the target acceleration is strictly white noise. Another simple model is the 'Wiener-process acceleration model' [60], where acceleration is modeled as a Wiener process. The latter approach is also referred to as the 'nearly-constant acceleration model.' Discussion on other models is available in [83]. We adopt a non-constant and adaptive acceleration model as described below. The model can adapt to necessary perturbation "gates" through parameter a_{max}.

Let the new state vector be $\bar{X}$=$[X_k \;\; \dot{X}_k]$, where $\dot{X}_k$ denotes the velocity of a particle at the k^{th} receiver. It is the rate of change of particles from the $(k-1)^{th}$ to the k^{th} receiver.

The state transition equations can be written as:

$$\dot{X}_k = \dot{X}_{k-1} + \gamma_{\mathbf{k}} ds_k \tag{4.1}$$

$$X_k = X_{k-1} + \dot{X}_{k-1} ds_k + \frac{1}{2}\gamma_{\mathbf{k}} (ds_k)^2, \tag{4.2}$$

where ds_k is a measure of distance between receivers k and $k-1$. Quantity ds_k can be constant with state or can vary (the latter is the case in our problem).

It is assumed that the target accelerates or decelerates: $\gamma_{\mathbf{k}} \in \mathbf{N}(\mathbf{0}, \mathbf{a_{max}})$ [83]. Parameter a_{max} is the maximum acceleration allowed in the motion of a particle and is defined to be the maximum change possible in the velocity/gradient of the particle. It is typically chosen empirically.

The state equation can be written in a matrix form:

$$\bar{X_k} = F\bar{X}_{k-1} + W(k), \tag{4.3}$$

where

$$\bar{X_k} = [X_k \;\; \dot{X}_k]^T, F = \begin{pmatrix} 1 & ds_k \\ 0 & 1 \end{pmatrix} \tag{4.4}$$

and

$$W(k) = \begin{pmatrix} \frac{(ds\gamma_{\mathbf{k}})^{\mathbf{2}}}{2} \\ ds \end{pmatrix}. \tag{4.5}$$

4.1.1 Error Analysis

Figure (4.2) demonstrates the performance of the PF that incorporates the gradient of arrival times in space. Again, the RMS error is plotted as a function of the number of particles. The new PF performs very well in both direct and SR arrival time estimation. It is worth noting that the SR arrival estimation is significantly superior than that of the simple model (Figure (3.5)). There is practically no error reduction for the direct arrival, because the original perturbations were adequate for that part of the problem.

The ML results, shown in Figure (3.5) as well, are superimposed on the PF error curves. The PF now outperforms the ML estimator consistently.

It should be noted that a Bayesian MAP estimator with uniform prior distributions such as those selected here for the PF initialization can only do as well as the ML processor; that is, the likelihood function and the posterior PDF are the same in that case (differing only by the constant of normalization). For this reason, the PF cannot do better outperform the ML approach at the first receiver; it can do worse, if the particles do not capture extensively the regions of interest of the likelihood. However, as the PF "collects" and explores information from arrival times in space, the results become increasingly better than those of the ML estimator. This is because the ML processor processes data in an isolated way, ignoring arrival times at neighboring hydrophones. Methods to improve the estimation process at the first receiver, and subsequently of the results at the whole array, will be discussed later in this work.

Figure (4.4) illustrates the PDFs of the arrival times computed using our PF method. The results suggest that, with inclusion of velocity/gradient in the model, the correct path for SR arrival can be identified effectively.

Calculation of PDFs is a significant asset of PFs. Instead of providing us only with point estimates used to calculate errors such as those of Figures(3.5) and (4.2), they provide PDFs that reveal the uncertainty in the estimation process. The breadth

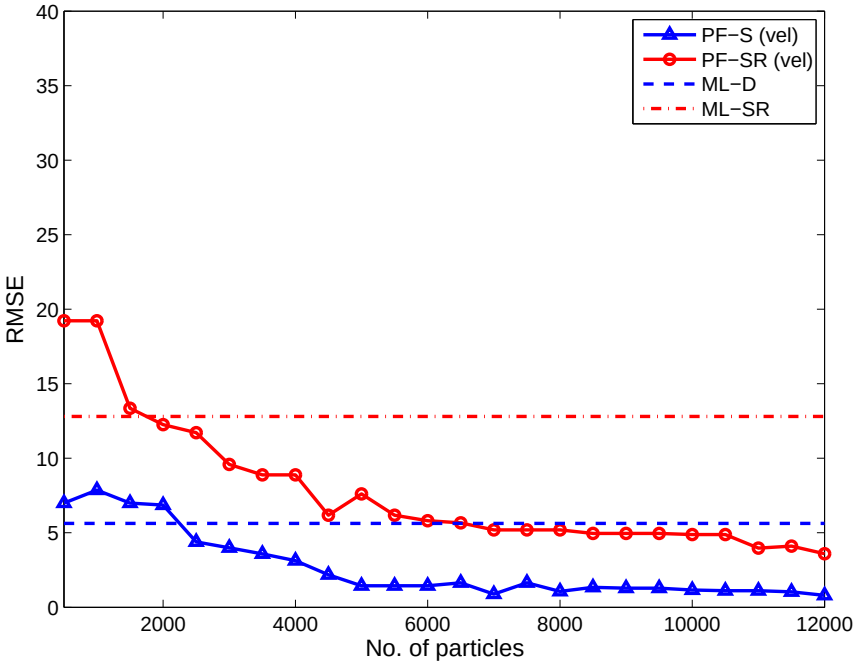

Figure 4.2 Performance of a PF with a velocity component (triangle: direct, circle: SR) and ML (dashed line: direct, dot-dashed line: SR). The SNR is 15 dB.

of the PDFs shows a measure of variance (which can be calculated), that quantifies a level of confidence one should have in particular point estimates. PDFs at receivers 2, 6, 10 and 11, for example, show increased uncertainty in comparison to those at other phones.

4.2 Particle Filtering for Tracking Signals with Unknown Amplitudes

In all our earlier discussions, the assumption of known amplitudes was made. This assumption is, however, not realistic. This section discusses a more scenario better reflecting reality by including amplitudes as unknowns. Since it has been established that the transition density function which includes the particle dynamics is better than the one which does not, we continue our discussion based on the new model.

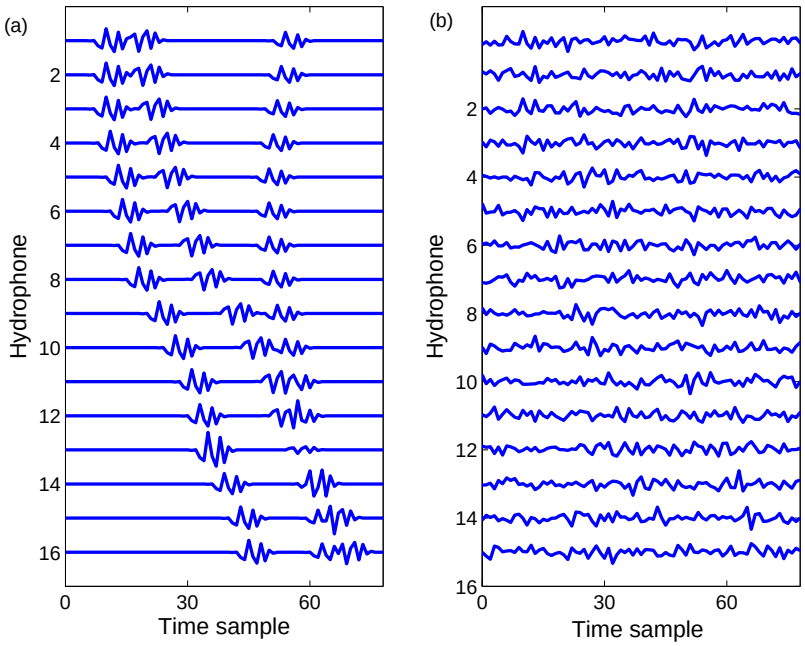

Figure 4.3 Noise-free receptions and one realization of noisy synthetic time-series with three arrivals.

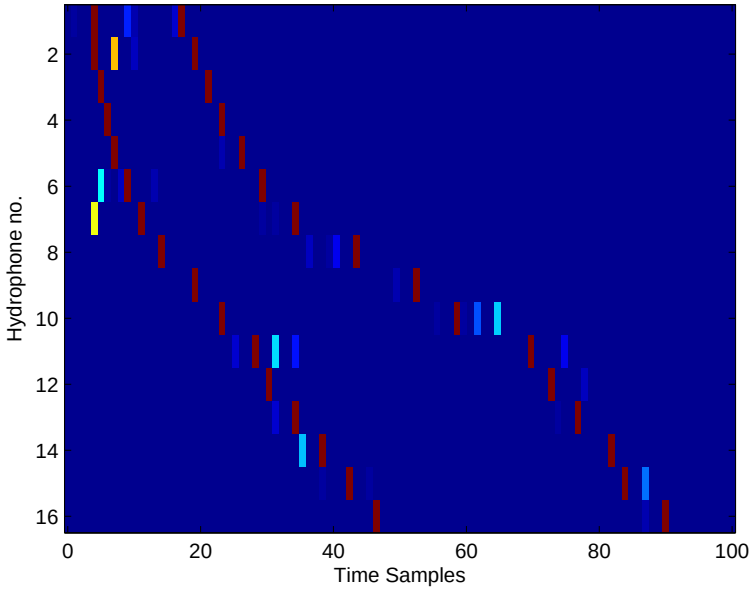

Figure 4.4 Arrival time PDFs for two paths using the dynamic model.

4.2.1 Model

Amplitude estimation can be treated in different ways. The first and most intuitive approach is to treat amplitudes as unknown parameters, including them in the state space and estimating them along with arrival times using particle filtering. Let ζ be the vector of all parameters describing the model:

$$\zeta_{\mathbf{k}} = [\bar{X}_k \quad a_k], \tag{4.6}$$

where a_k is the vector of amplitudes associated with particle X_k and $\bar{X}_k$ is vector $[X_k \ \dot{X}_k]$. Amplitudes are assumed to follow the following propagation model:

$$a_k = a_{k-1} + w, \tag{4.7}$$

where w is additive Gaussian noise with mean 0 and variance σ_w^2. Amplitude particles can be sampled according to [84]:

$$a_k^i \sim N(a_{k-1}^i, \sigma_w^2). \tag{4.8}$$

Following the sampling process of the time particles as per Equation (4.1) and their respective amplitudes as per Equation (4.8), the likelihood is computed for the selected samples for X_k and a_k. Weights are then calculated for these particles. This approach will increase the computational load of the PF process by doubling the state vector dimension, thus necessitating a larger number of particles.

Alternative approaches for the estimation of amplitudes have been discussed

in [54, 85, 86]. In [85, 86], amplitudes do not enter the vector of unknown parameters but instead can be estimated using an ML or MAP estimator (since ML and MAP generate the same estimate for uniform priors). Because the conditional PDFs of amplitudes on arrival times follow a Gaussian distribution, estimation is straightforward. We use the approach of [45, 85, 86] to estimate amplitude modes conditional on the arrival time particles. We can also trace the covariance matrix of these conditional PDFs [85, 86]. Since these conditional PDFs are Gaussian, we have enough information to draw samples from those. These samples will be used for the construction of the marginal posterior PDFs of the amplitudes at each state. The modes are used at the next state for the prediction of the new set of arrival times and amplitudes. Specifically [45]:

$$A = \Lambda^{-1}\phi, \tag{4.9}$$

where ϕ_p is a column vector with $\phi_p = \sum_{t=1}^{N_s} s(t-\tau_p)Y(t)$, $p = 1, \ldots, P$, (Y is the received time-series) and A is the column vector of unknown amplitudes. Also,

$$\Lambda = \begin{pmatrix} \lambda_{11} & \lambda_{12} & \ldots & \lambda_{1p} \\ \lambda_{21} & \lambda_{22} & \ldots & \lambda_{2p} \\ \ldots & \ldots & \ldots & \ldots \\ \lambda_{p1} & \lambda_{p2} & \ldots & \lambda_{pp} \end{pmatrix}, \tag{4.10}$$

where $\lambda_{ij} = \sum_{t=1}^{N_s} s(t-\tau_i)s(t-\tau_j)$, $i, j = 1, \ldots, P$.

This approach requires fewer particles than the method including amplitudes in the state vector. This is because the PF efficiency largely depends on the dimension of the state vector [78] as emphasized so far: more unknowns require more particles. Under some circumstances, the number of particles can also be reduced by using

Rao-Blackwellization [87, 56]. The idea is to separate the state variables, if possible, and use a KF for the estimation of part of the state vector when linearity and normality permit. A PF is only employed for the remaining part of the state vector.

4.2.2 Error Analysis

The performance of PF with the addition of unknown amplitudes is depicted in Figure (4.5). Errors with unknown amplitudes are slightly larger than errors with known amplitudes, which is expected. The comparison between PF and ML errors still demonstrates a remarkable gain in using a PF over ML.

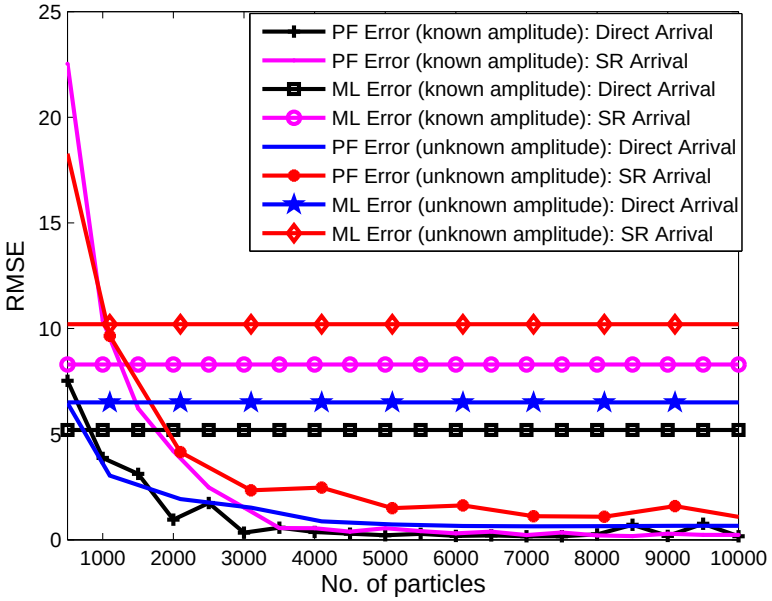

Figure 4.5 Comparison of PF estimation with known and unknown amplitudes for an SNR=17 dB. ML estimates are superimposed.

4.2.3 PDF Estimation

This section goes beyond the error analysis and characterizes arrival times and their amplitudes by estimating their PDFs. By studying the estimated PDFs, one can

estimate statistical characteristics such as mean and mode of the unknown parameters and variance within the estimation process.

4.2.3.1 Case 1: Synthetic Data. This case estimates for the time-series shown in Figure (4.3). The signal of Figure (4.3(a)) is noise-free and includes arrivals three paths now: direct, SR and BR. The SR and BR paths cross; a noisy realization is shown in Figure (4.3(b)). The challenge in identifying multipath arrivals is that, at some point, paths may be very close (practically coinciding in some cases). Many time delay methods are unable to identify arrivals when they are close together and instead might perceive them as one single echo. Applying a PF, we estimate the different arrival times and their posterior PDFs (initially, under the assumption of a known number of paths). The power of this method lies in the sequential Bayesian framework that allows us to distinguish between two crossing paths, albeit with significant uncertainty. The arrival time PDFs illustrated in Figure (4.6(a)) reveal the effectiveness of the method in resolving successfully the crossing paths. The amplitude PDFs are demonstrated in Figures (4.6(b), (c), and (d)) for receiver 12 for the direct path, SR, and BR, respectively. It is noteworthy that the PDFs are multimodal and show an extensive spread at the 12^{th} receiver, where the SR-BR paths approach each other significantly.

4.2.3.2 Case 2: Haro Strait Data. For the experiment set up, an array of 16 hydrophones was deployed. The vertical spacing between phones was 6.25 m apart with the exception of the spacing between phones eight and nine which double. The shallowest receiver was about 30m from the surface. The acoustic source was a household light bulb. Data were collected at a sampling rate of 1750Hz. The experiment was also described in Chapter 2. The signal received at the hydrophones

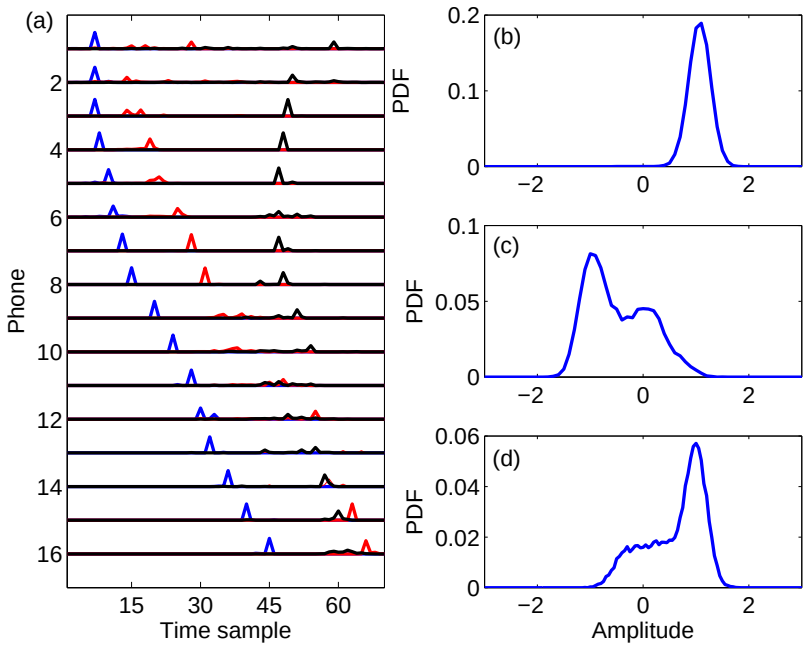

Figure 4.6 (a) Posterior PDFs of arrival times for synthetic data. (b) Amplitude PDFs at phone 12.

is shown in Figure (4.7) and the results of estimation of arrival time PDFs using the PF are shown in Figure (4.8). A spread of about two samples is noticed in the estimation of arrival times; the PF process, however, has clearly estimated the arrivals effectively. Relatively to other receivers, the PDF has a larger spread at the last two receivers, where the SR and BR arrivals are in close proximity.

4.3 Initialization

A PF is an MCMC (Markov Chain Monte Carlo) method that updates particles drawn at a previous state. It strongly relies on the accuracy of the posterior PDF estimation at the first state . If the initial sample set, selected often from a uniform distribution before updating (no prediction is feasible) does not capture the true PDF of the unknowns, then the error propagates into the following states and the updated cloud will carry for a few states the error at state 1. A useful initial sample set is realizable if the initial sample is drawn from an informative space or if numerous

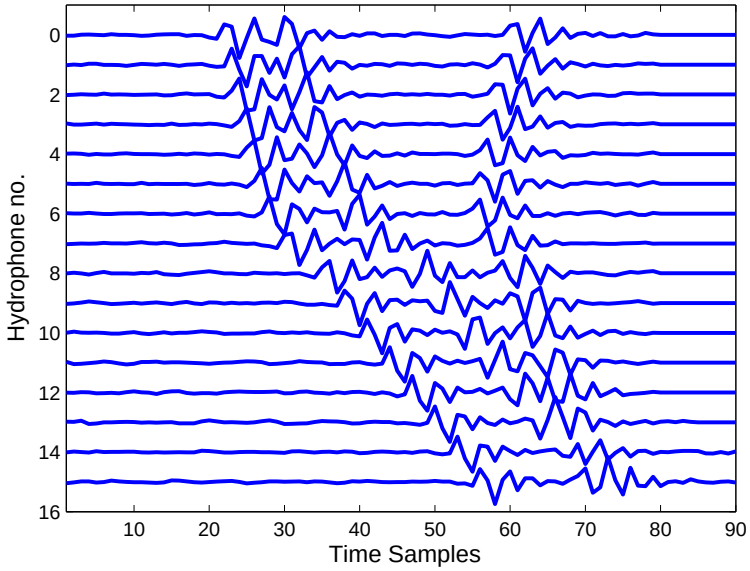

Figure 4.7 Received time-series at a tilted vertical line array from the Haro Strait Primer experiment.

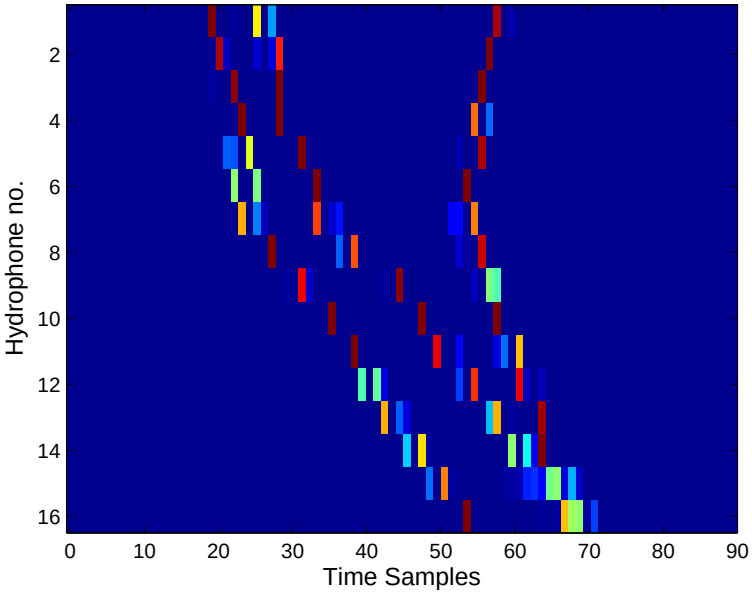

Figure 4.8 PDFs of arrival times extracted from Haro Strait data.

particles are drawn at state 1.

The order of complexity for a PF is $O(N)$ as previously discussed. If the number of particles is large, as just indicated, the complexity may be prohibitive. Alternatively, the number of samples only for the first state can be large and can be reduced later on. For initializing the first particle set, N samples are drawn from a uniform distribution over the entire search space as has been discussed. To enhance the PF performance we can initially select M particles, also from a uniform distribution, where $M > N$. We then select at the end of the first state the N particles with the highest probability. This not only keeps the computational requirements at a reasonable level but also improves the performance of PF, as can be noticed by comparing Figures (4.9) and (4.10). The former demonstrates results from arrival time estimation from time-series with four arrivals when N is constant. The latter illustrates results from the same time-series when M particles are selected at state (phone) 1.

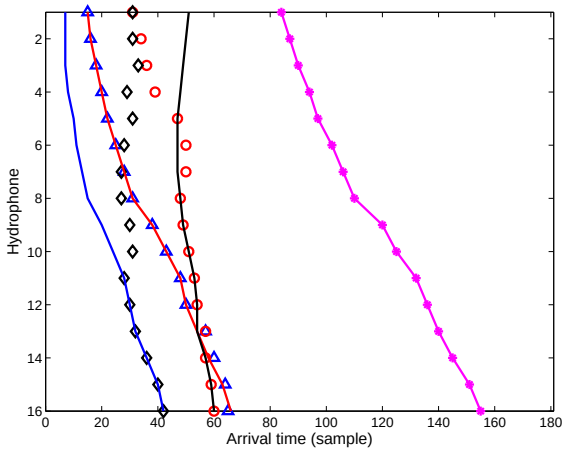

Figure 4.9 Arrival time estimation with N particles at all states. Straight lines demonstrate the true arrival tracks. Triangles, circles, diamonds, and asterisks show the estimates for the direct, SR, BR, and first sediment-halfspace interface reflection.

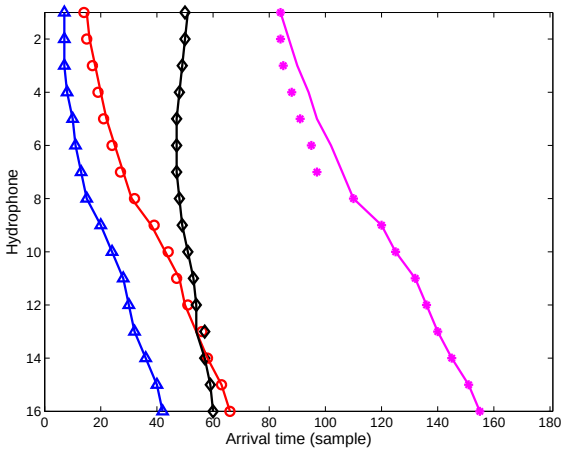

Figure 4.10 Arrival time estimation with M particles at state 1 and N particles $N < M$ at subsequent states. Straight lines demonstrate the true arrival tracks. Triangles, circles, diamonds, and asterisks show the estimates for the direct, SR, BR, and first sediment-halfspace interface reflection.

CHAPTER 5

UNKNOWN NUMBER OF ARRIVALS

5.1 Introduction

In our work, the number of arrivals has been assumed to be fixed and known, that is, the state-space estimates calculated so far have been conditional on the number of arrivals. In practical applications, this information is not available. Hence, the assumption of a known and fixed number of arrivals needs to be relaxed. This makes the dimension of the model unknown at every receiver. When the number of targets (arrivals, in our case) is known and constant, the state-space is just the collection of all individual target states, but when the targets are allowed to enter or leave the area under consideration, the dimensionality of the state-space is determined at every step by the number of targets present. Hence, the variable target motion model should not only serve to predict how targets will move, but it should also predict the probability of how many targets/arrivals are present within the examined time-frame.

The signal processing and information literature contains a number of approaches to the problem of determining the number of paths within a data set. In [88], the order α of the model was considered as a random variable and it was estimated along with arrival times, amplitudes, and noise variance. This was based on work presented in [89], where the number of parameters to be estimated in problems similar to ours was estimated using the Akaike Information Criterion (AIC) and the Schwartz-Rissanen Criterion (SRC, also known as Minimum Description Length or MDL). In addition to the calculation of point estimates for the number of arrivals, posterior PDFs for that number were also computed in [88], expressing the uncertainty in the estimation of α. The method discussed in [88] assumed a uniform prior for the

number of sources over a range believed to be realistic and estimated the number of paths at every receiver individually; no information was shared across receivers. In this work, we use the information available on the number of paths at the k^{th} phone to estimate the number of paths at the $k+1^{th}$ receiver. In this manner, the dimension of the model is allowed to change at every state based on knowledge on the number of paths from the preceding state.

5.2 The Model

Let η be a vector containing all unknown parameters within a state - arrival times, amplitudes, and order of the model:

$$\eta = (\bar{X}^{\,i}_{k(\alpha^i_k)}, a^{\,i}_{k(\alpha^i_k)}, \alpha^i_k), i = 1, ..., N. \tag{5.1}$$

A transition density matrix $P_{tr} = [\pi_{ij}]_{\alpha_{max} \times \alpha_{max}}$ is introduced [56]; α_{max} is the maximum number of paths assumed to be present in a time frame, π_{ij} is the probability of movement from state i to state j, $i, j = 1, \ldots, \alpha_{max}$ and $\sum_j(\pi_{ij}) = 1$.
We initially assume that the maximum number or arrivals that can exist in a given time frame is two; then $\alpha_k = [1, 2]$ and the transition density matrix can be written as:

$$P_{tr}(\alpha_k|\alpha_{k-1}) = \begin{pmatrix} pr_{11} & pr_{12} \\ pr_{21} & pr_{22} \end{pmatrix}. \tag{5.2}$$

This means that, if the model order is *one*, it will continue to be one with probability pr_{11} at the next state. Alternatively, the number of arrivals can increase to two at the next state with probability pr_{12}. On the other hand, if the model order is two at the present state, that is, there exist two arrivals, there is a probability of pr_{21} that

at receiver k an arrival moves out of the window and a probability of pr_{22} that the signal continues with two arrivals. Matrix P_{tr} does not have to be symmetric.

Estimation of model order is a tricky issue that requires careful attention. Considering our case, we assume for a moment that we have a time-series with one arriving path with an amplitude of one. We can create infinitely many combinations of multiple paths with the exact same arrival time and amplitudes that, superimposed, will generate the true reception. The model with the highest order is the one that will prevail, because, in a noisy environment, when using more paths we will be able to replicate better the existing signal. In our example, the larger model order possible (two in this example) will always be preferred. That is, there is an inherent bias towards large orders. In the derivation of AIC and SRC, terms were added to the main selection component to penalize for order, so that the best match with the smallest order was selected. Within the Bayesian framework that we follow here, the penalizing term occurs naturally by forming the posterior PDF based on the likelihood and priors, as follows.

Once a transition matrix has been selected, following the work of [88], we select uniform priors on arrival times and amplitudes:

$$p(a_{kp}) = 1 \tag{5.3}$$

$$p(X_{kp}) = \frac{1}{N_s}. \tag{5.4}$$

The likelihood at a specific state has already been derived in Equation 3.25. Only there, as just mentioned, the number of arrivals P was assumed to be known. The joint prior for all arrival times $\frac{1}{N^p}$ (resulting from the multiplication of the single arrival priors) was omitted because it was the same for all states. Now that the assumption of a known and constant model order is relaxed, this term becomes essential in the posterior PDF formulation:

$$p(Y_k \mid X_k) \propto \frac{1}{N_s^p} \exp(-\frac{\sum_{n=1}^{N_s}(Y_k - \sum_{p=1}^{P} a_{kp} s(n - X_{kp}))^2}{2\sigma^2}). \tag{5.5}$$

The term $\frac{1}{N_s^p}$ is here the penalizing factor. For large values of p, this term has a small value associating with it a small probability. Small values of p are associated with higher probability.

5.2.1 Results for an Unknown Number of Arrivals

5.2.1.1 Synthetic Data. A synthetic case was developed to study the effect of an unknown and varying order. Figure (5.1(a)) shows a noise-free signal that initially has two arrivals. The SR arrival gradually moves out of the observation window and only one arrival remains at receivers 12 through 16. Results on arrival time estimation using the transition model are shown in Figure (5.1(b)). In Figure (5.2), we show the PDF for order α. We notice that the probability of order two is dominating at receivers one through 11. There is a noticeable switch at receiver 12, where the probability for the order to be one is higher than the probability corresponding to an order of two. This implies that our estimator was successful in detecting that one of the signals has moved out of the window of observation at receiver 12. For this example, an assumption of $\alpha_k = [1, 2]$ was made. The transition matrix was:

$$P_{tr} = \begin{pmatrix} 0.75 & 0.25 \\ 0.25 & 0.75 \end{pmatrix}. \tag{5.6}$$

Because the model can jump or switch between order values, the method is also referred to as a jumping or switching model.

The example with three arrivals previously presented was also examined here from the perspective of the estimation of the number of paths. Figure (5.3) presents the, now truncated, time-series; the second and third arrivals exit the observation window at receiver 13. Figure (5.4) demonstrates the point estimates obtained by the PF superimposed on the true tracks. Only at the first phone, one of the arrivals (SR) is missed and the order is incorrectly determined as seen from the PDF of Figure

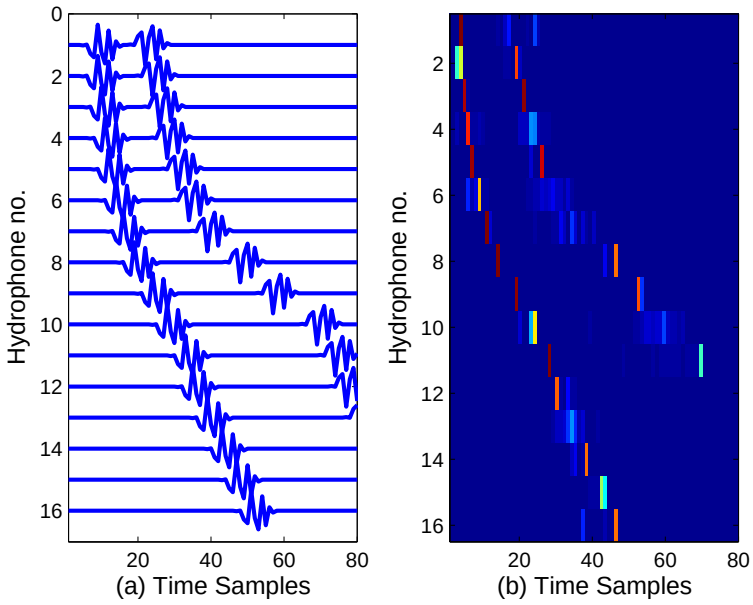

Figure 5.1 (a) Noise-free signal showing transition of an arrival out of the time window (b) PDF of arrival times.

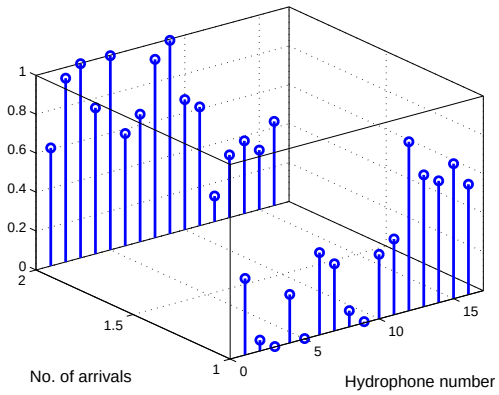

Figure 5.2 PDF of the number of arrivals.

(5.5). For all other receivers up to and including receiver 11, the order is estimated correctly as three. After the 11^{th} phone, the probability is concentrated at $\alpha = 1$.

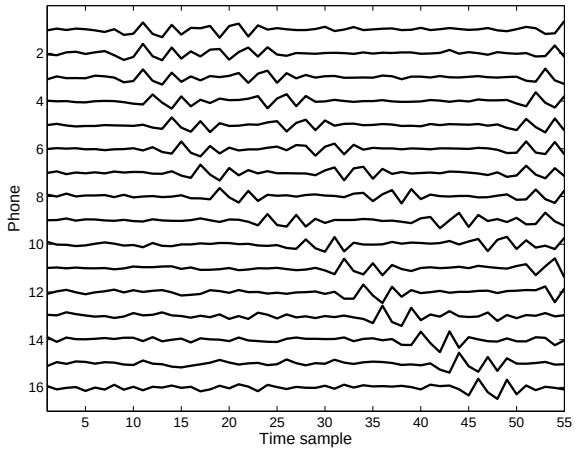

Figure 5.3 Noise free signal showing the number of arrivals decreasing from three to one.

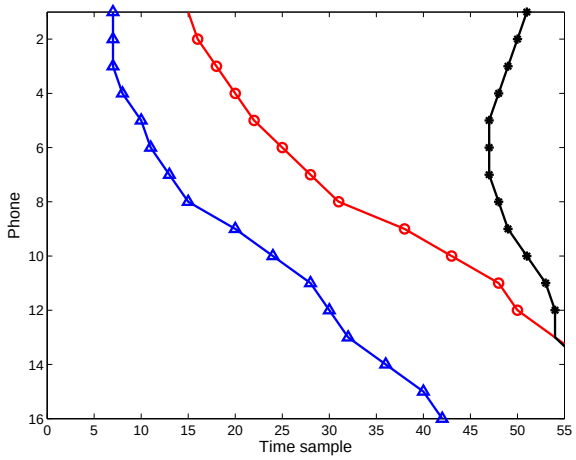

Figure 5.4 Estimates of direct, SR, and BR arrival times for an unknown number of arrivals superimposed on the true tracks.

5.2.1.2 Real Data Results: The Haro Strait Experiment. The signal shown in Figure (5.7(a)) is a set of receptions from the Haro Strait Primer experiment. Figure (5.7(b)) demonstrates the corresponding arrival time PDFs when the number

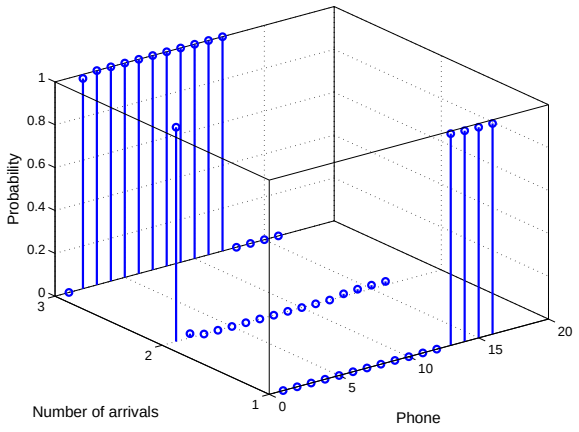

Figure 5.5 PDF of the number of arrivals; the order changes from three to one.

of arrivals is unknown. The arrivals seem to have been estimated well although more uncertainty was introduced, namely the number of paths was here unknown. The assumption was that $\alpha_k = [1, 2, 3, 4]$. Figure (5.6) suggests a significant probability for the presence of three arrivals, which is the true case, with little probability for orders of two or one. A rather small, but not negligible, probability is also associated with four arrivals. The transition matrix used was:

$$P_{tr} = \begin{pmatrix} 0.4 & 0.2 & 0.2 & 0.2 \\ 0.2 & 0.4 & 0.2 & 0.2 \\ 0.2 & 0.2 & 0.4 & 0.2 \\ 0.2 & 0.2 & 0.2 & 0.4 \end{pmatrix}. \tag{5.7}$$

This simply means that the probability of the order remaining the same is 0.4; the probability of switching to a different order is 0.2.

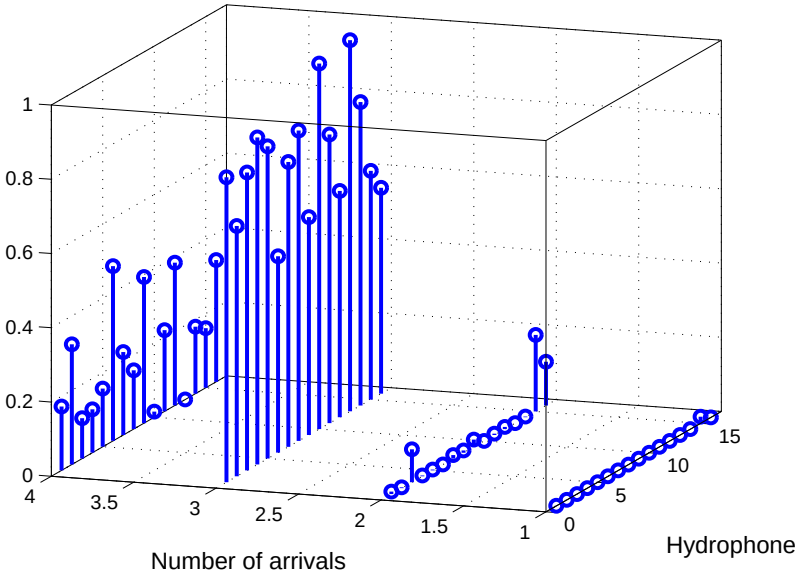

Figure 5.6 PDF of the number of arrivals α for Haro Strait data.

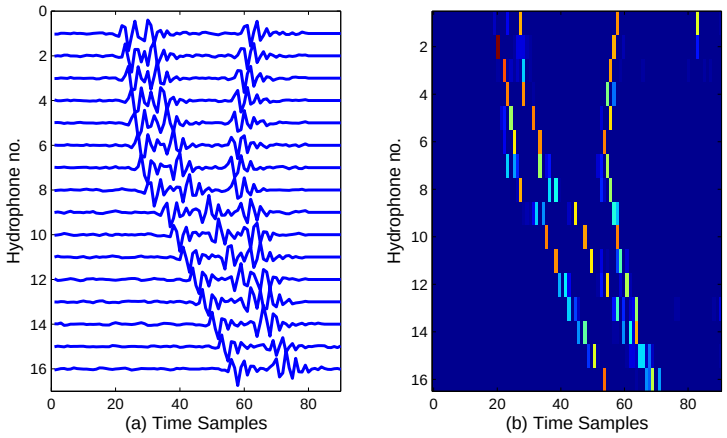

Figure 5.7 (a) Signal from the Haro Strait experiment; (b) PDF of arrival times when the number of arrivals is unknown.

CHAPTER 6

BAYESIAN FILTERING: SMOOTHING

6.1 A Smoothing Particle Filter

The quality of PF estimates largely relies on initialization as previously discussed. In many cases, estimates for advanced states in time or space are excellent, with the estimates at initial states suffering from inaccuracies. There is no reason, however, not to exploit information from advanced states (deeper receivers, in our case) to improve the estimates at the initial (shallower) ones. This process is typically referred to as smoothing, because it "smooths out" volatility in the estimation process. The main objective is to improve the standard particle filter by adding backward steps.

In [90], use of joint densities was proposed for filtering and smoothing, that is, using $p(q_t, q_{t-1}|Y_t)$ for filtering and $p(q_{t+1}, q_t|Y_T)$ for smoothing. The advantage of the method is that particles are sampled from a proposal density which incorporates information both from the previous and the next receiver. Thus, even if estimation at a previous receiver is erroneous because, for example, of a low SNR, information from the $(k+1)^{th}$ receiver can be used to correct the estimation at the k^{th} receiver.

A fixed interval smoothing method for Markovian switching systems is studied in [91]. The algorithm used two multiple-model filters, where the MAP-smoothed estimate of X_k was computed using a combination of both a forward and a backward MAP estimate.

Another approach was suggested in [92], which relies first on a forward filter and then a backward smoothing pass. We describe here this latter approach, which we adapted to our problem.

Density $p(X_k|Y_{1:k})$ is updated as follows:

$$\begin{aligned} p(X_k|Y_{1:k}) &\propto p(Y_k|X_k)p(X_k|Y_{1:k-1}) && (6.1) \\ &= \int p(Y_k|X_k)p(X_k|X_{k-1})p(X_{1:k-1}|Y_{1:k-1})dX_k. && (6.2) \end{aligned}$$

On the same lines, smoothing can be achieved by moving backwards in space recursively as:

$$p(X_k|Y_{1:L}) = \int p(X_{k+1}|Y_{1:L})\frac{p(X_{k+1}|X_k)p(X_k|Y_{1:k})}{p(X_{k+1}|Y_{1:k})}dX_{k+1}. \quad (6.3)$$

Smoothing is achieved as follows:

1. Select a particle $\tilde{x}_{k+1}^j$ at receiver $k+1$
2. Compute $w_{k|k+1}^i \propto w_k^i f(\tilde{x}_{k+1}^j|x_k^i)$ for $i = 1, \ldots, N$
3. Choose $\tilde{x}_k = x_k^i$
4. $\tilde{x}_{1:16} = [\tilde{x}_1, \ldots, \tilde{x}_{16}]$ is one new realization from the posterior joint PDF of all unknowns.

If we perform the process many times (let's say N), item 4 of the algorithm will produce N realizations of the joint posterior PDF of times and amplitudes. This PDF shows significantly decreased uncertainty in comparison to the original one obtained by only using a forward filter. It should be also noted that:

- This process improves the estimates at the first phone, because now there is a prior history (from phone 2) that is propagated backward.

- The complexity of the approach does not increase, because no more particles are selected and resampling (which is computationally intensive) is not performed when moving backwards. The method still has order of complexity $O(N)$ [92].

6.2 Results

Smoothing offers a significant advantage in our case, as demonstrated in Figure (6.1). The figure shows (a) a comparison of PFs with and without smoothing for an SNR of 13 dB and (b) a comparison of a smoothing PF with the standard ML estimator in (b). Results were obtained via a Monte Carlo performance evaluation process with $N_r = 100$ noisy realizations. Five-hundred multi-dimensional particles were drawn from each state during the backward step of the smoother. RMS errors are plotted against the number of particles. The top figure confirms that the smoothing filter reduces the estimation error. For example, the RMS error for the third path (green curve with asterisks) is reduced approximately by 50% when the smoother is used (from eight to four - green error curve with circles). The second path error is also reduced and so is the direct arrival error (reduction of the latter error is not very clear in the figure because the original, forward-only PF error was small to begin with). We had already established that the PF with the kinematic constraint is significantly superior to the conventional ML estimator. The new PF has an even bigger advantage, as illustrated in Figure (6.1(b)).

Even more impressive are the results shown in Figure (6.2). Figure (6.2(a)) shows the posterior PDF of the arrival time of the BR path at the third phone computed via a conventional forward PF. Figure (6.2(b)) presents the corresponding PDF after the smoother. The true arrival time sample is 49. The top PDF is multimodal with probability density spread over a range between 48 and roughly 60. The PDF after smoothing has all its probability around the true arrival time.

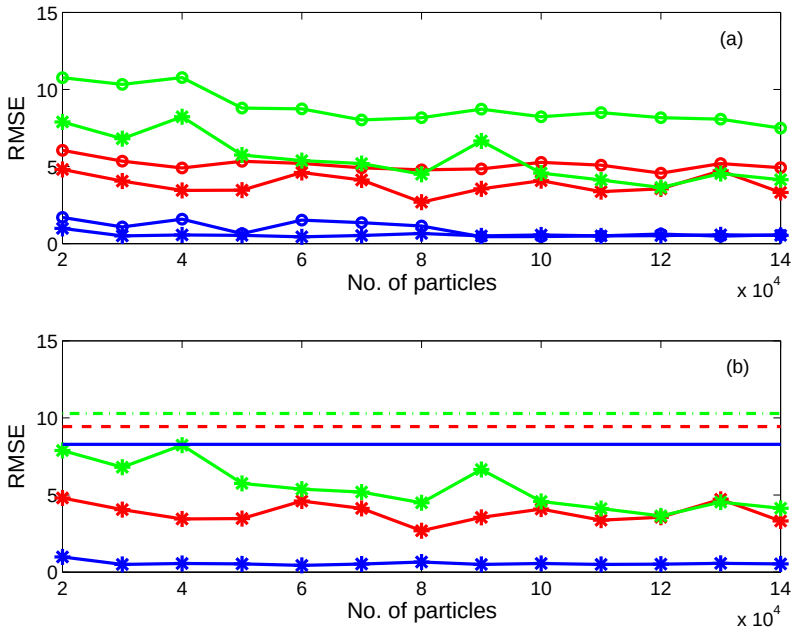

Figure 6.1 Demonstration of the advantage of a PF with smoothing over a simple PF for three paths at an SNR of 13 dB: (a) RMS errors for arrivals times from a forward PF for three paths (o) and a forward-backward filter for the same paths (*); (b) RMS errors for arrivals times a forward-backward filter for the three paths (*) and ML RMS errors (lines).

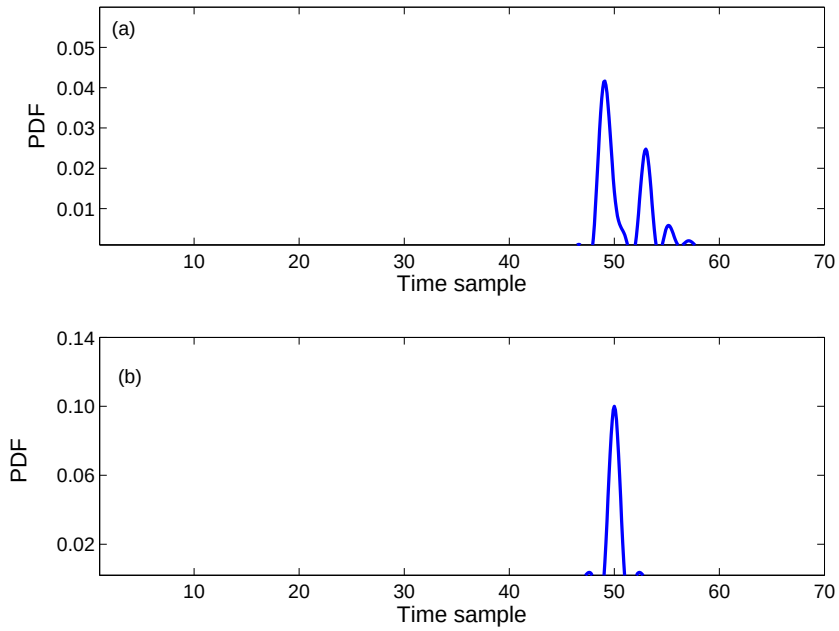

Figure 6.2 (a) PDF of the SR path arrival time at the first phone with the conventional forward PF. (b) PDF of the SR path arrival time at the first phone with the smoothing PF.

CHAPTER 7

UNCERTAINTY ANALYSIS

As mentioned earlier in Section 1.4, quality in geometric and environmental inversion depends on the accuracy in the estimation of arrival times. In this section, our focus is on performance assessment and quality evaluation of PFs through the study of uncertainty of extracted parameter estimates associated with sound propagation.

If $\mathbf{m}$ is the vector of model parameters and $\mathbf{d}$ is the vector of observed data, then, under the Bayesian framework, the posterior PDF $p(\mathbf{m}|\mathbf{d})$ is given by:

$$p(\mathbf{m}|\mathbf{d}) = \frac{p(\mathbf{d}|\mathbf{m})p(\mathbf{m})}{p(\mathbf{d})}, \tag{7.1}$$

where $p(\mathbf{d}|\mathbf{m})$ is the likelihood and $p(\mathbf{m})$ contains the prior information available on model parameters.

Uncertainty analysis along these lines is carried in [93, 94, 25, 95] for matched-field inversion. Specifically, in [25, 95], a fast GS approach is employed for estimation of the multi-dimensional integral of the PDF described in Equation (7.1). Sen and Stoffa [96] investigate the performance of several techniques like Gibbs Sampling, Simulated Annealing, and Genetic Algorithms for the evaluation of joint and marginal posterior PDFs.

We apply the PF method to extract arrival times with their respective amplitudes from a received set of signals and the results are used as input to an inversion approach similar to that of Chapter 2, that produces posterior PDFs as just described. It is particularly important to propagate the estimates of the arrival time PDFs through the inversion process, so that we can study the uncertainty that is reflected in our

final inversion results. The PDF $p(\mathbf{m}|\mathbf{d})$ is computed at each point in the observed data $\mathbf{d} = \mathbf{d_{obs}}$ where $\mathbf{d_{obs}}$ is the set of estimated data features - here arrival times.

Figures (7.1, 7.2) compare the uncertainty in inversion associated with the ML and PF arrival time estimation processes applied to synthetic data, designed to closely simulate the Haro Strait experiment. The true values are 400 m, 50 m and 190 m, for horizontal range, source depth, and ocean depth, respectively.

The estimation process was as follows. We estimated arrival times using a MAP (identical to ML for our priors) approach at isolated receivers with a method such as GS-MAP. Along with the MAP estimates, we also produced the posterior PDFs of the arrivals. In parallel, we also estimated the same arrival times and their corresponding PDFs with our PF method, which accounted for time evolution across hydrophones. Through our studies in the previous chapters, we have established that the latter approach produces smaller errors. The "tighter" estimates produced by the PF reflect into the range, source depth, and water column depth estimation process. Figures (7.1(a)) and (7.1(b)) present posterior PDFs for ocean depth and source-receiver distance using the GS-MAP approach and the PF approach, respectively. The inversion employing PF arrival time estimates is characterized by significantly reduced uncertainty in comparison to the inversion process relying on simple GS-MAP estimates, evidenced via the small spread (variance) of the PDF in the former case. Similar observations are made by observing Figures (7.2(a)) and (b), illustrating posterior PDFs of range and source depth.

Inversion results from the application of our algorithm to Haro Strait data are presented in Figures (7.3-7.5). These figures portray the uncertainty in the estimation of horizontal range of first receiver vs. ocean depth and horizontal range of first receiver vs. source depth. The results are in agreement with the benchmark values of the parameters.

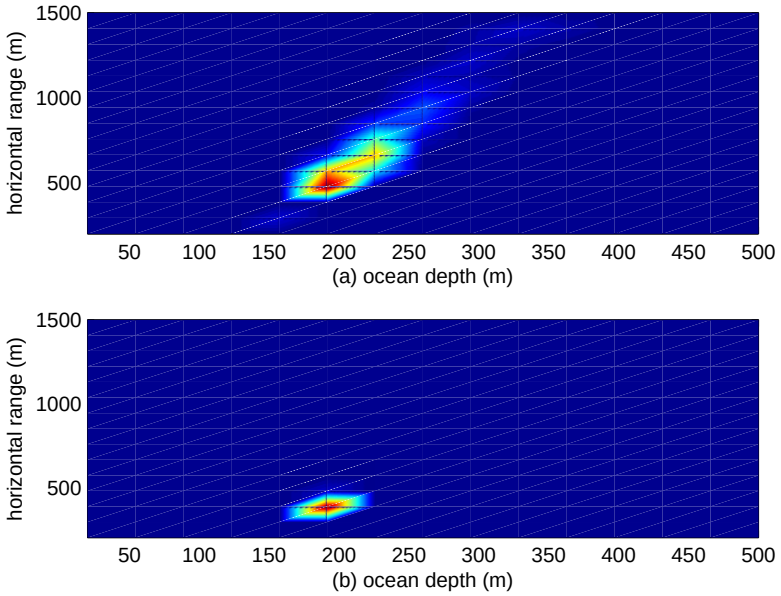

Figure 7.1 Uncertainty comparison for ML estimation vs. PF estimation at an SNR of 17 dB where (a) shows the uncertainty associated with estimation of ocean depth and horizontal range using ML and (b) illustrates the uncertainty in estimation when PF estimates are used.

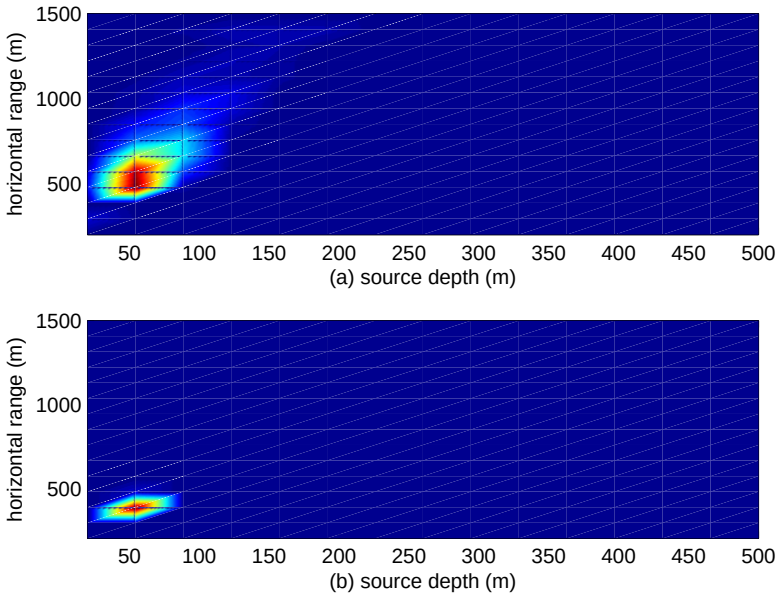

Figure 7.2 Uncertainty comparison for ML vs. PF estimation at an SNR of 17 dB where (a) shows the uncertainty associated with estimation of source depth and horizontal range using ML and (b) illustrates the uncertainty in estimation when PF estimates are used.

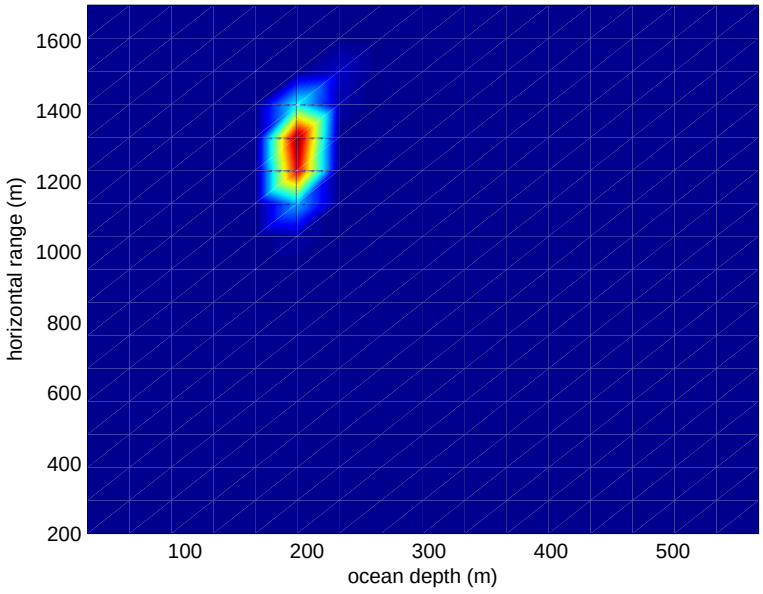

Figure 7.3 Posterior PDFs of source depth and horizontal range for Haro Strait data.

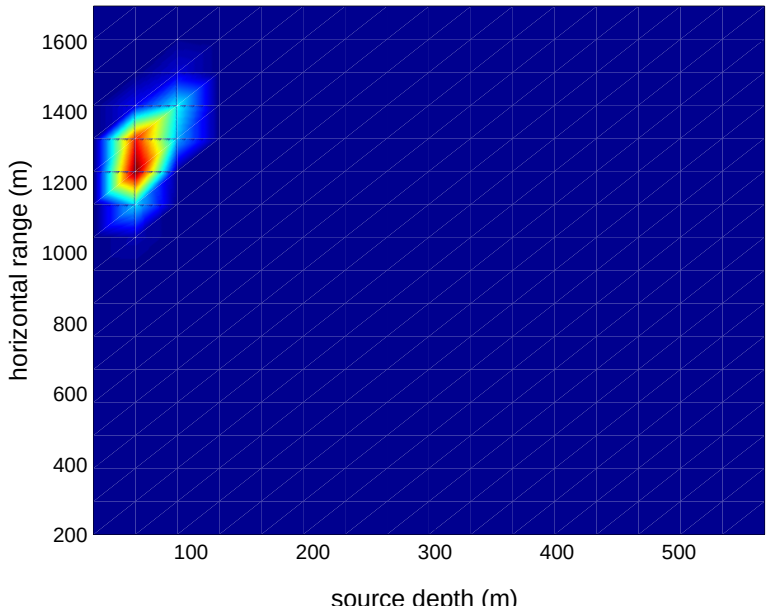

Figure 7.4 Posterior PDFs of ocean depth and horizontal range for Haro Strait data.

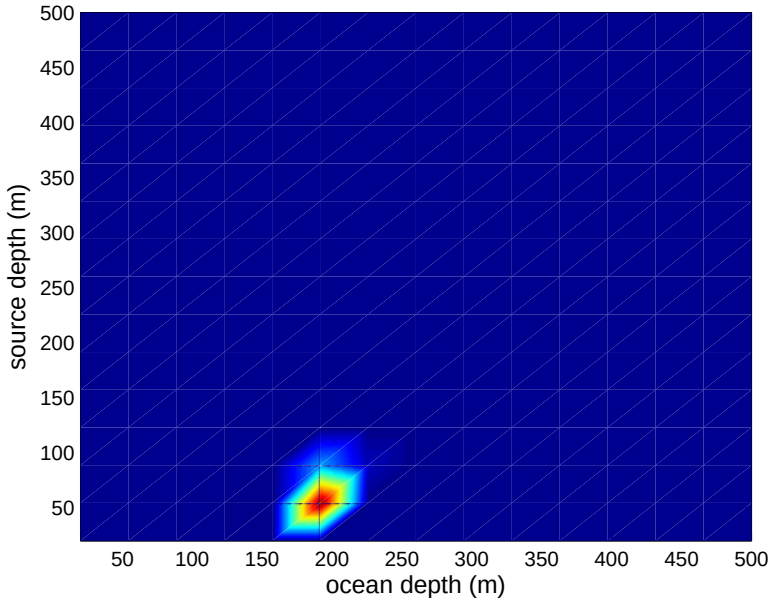

Figure 7.5 Posterior PDFs of ocean depth and source depth for Haro Strait data.

CHAPTER 8

CONCLUSIONS AND FUTURE WORK

In this work, we developed an estimator for dynamically tracking arrival times in space. This work is novel, because, to date, arrival time estimation (or time delay estimation, as it is often referred to) has been performed at one phone at a time. Our method relies on sequential Bayesian filtering, namely particle filtering. It produces not only estimates of arrival times of specific sound rays propagating in an ocean environment along with their corresponding amplitudes, but it also estimates joint PDFs for those quantities. The essence of the method is the use of arrival time PDFs at one phone for estimation of arrival times at the subsequent hydrophone location.

The method was evaluated through a comparison to a standard ML estimator. Via a Monte Carlo performance evaluation process, we initially found out that, under some circumstances, the method was not as effective and consistent as the ML estimator. To resolve this problem, we developed a new approach that also estimated and incorporated the gradient of arrival times. This latter approach was found to have a significant advantage over the ML method. As expected, this advantage depended on the number of samples employed by the PF process.

We also found out that the performance of the PF method strongly depended on the estimates at the first phone. At that location there is no prior information from previous phones and the estimates may be poor because of undersampling of the search space. To address that, many particles would typically be required, increasing the computational complexity of the method. We resolved this problem by considering a filter with many particles at the initial state, out of which fewer particles were retained for estimation at the following phones. Results for four arrivals demonstrated the power of the method. Smoothing is another factor that played an important role

in the quality of the estimates, significantly reducing RMS errors.

In the future, we plan to use both the arrival time estimates obtained with the PF and the corresponding amplitudes extracted from real data to perform more detailed geometry estimation and geoacoustic inversion. We can obtain more information on sound velocities and attenuation; the latter is strongly dependent on arrival amplitudes. Thus, we may be able to extract useful information on sediment properties. Also there are ways that can help us improve the estimation of the number of arrivals, by generating a more flexible approach that will allow us to remove arrivals that are weak and may not provide accurate information on inversion. This is a topic that will be further investigated.

BIBLIOGRAPHY

[1] A. Tolstoy, *Matched Field Processing for underwater acoustics*. World Scientific, 1993.

[2] S. E. Dosso, M. L. Yeremy, J. M. Ozard, and N. R. Chapman, "Estimation of ocean-bottom properties by matched-field inversion of acoustic field data," *IEEE Journal of Oceanic Engineering*, vol. 18, pp. 232–239, 1993.

[3] R. M. Hamson and R. M. Heitmeyer, "Environmental and system effects on source localization in shallow water by the Matched-Field processing of a vertical array," *J. Acoust. Soc. Am.*, vol. 86, pp. 1950–1959, 1989.

[4] Z.-H. Michalopoulou and M. B. Porter, "Matched-Field processing for broad-band source localization," *J. Acoust. Soc. Am.*, vol. 21, pp. 384– 392, 1996.

[5] A. Tolstoy and O. Diachok, "Acoustic tomography via matched field processing," *J. Acoust. Soc. Am.*, vol. 89, pp. 1119–1127, 1991.

[6] R. K. Brienzo and W. S. Hodgkiss, "Broadband Matched-Field processing," *J. Acoust. Soc. Am.*, vol. 94, pp. 2821–2831, 1993.

[7] A. B. Baggeroer, W. A. Kuperman, and P. N. Mikhalevsky, "An overview of Matched Field methods in ocean acoustics," *IEEE Journal of Oceanic Engineering*, vol. 18, pp. 401–424, 1993.

[8] Z.-H. Michalopoulou, "The effect of source amplitude and phase in matched field source localization," *J. Acoust. Soc. Am. Exp. Lett.*, vol. 119, pp. EL21–EL26, 2006.

[9] A. B. Baggeroer, W. A. Kuperman, and H. Schmidt, "Matched Field processing: Source localization in correlated noise as an optimum parameter estimation problem," *J. Acoust. Soc. Am.*, vol. 83, pp. 571–587, 1988.

[10] S. E. Dosso, M. R. Fallat, B. J. Sotirin, and J. L. Newton, "Array element localization for horizontal arrays via occams inversion," *J. Acoust. Soc. Am.*, vol. 104, pp. 846–859, 1998.

[11] Z.-H. Michalopoulou and X. Ma, "Source localization in the Haro Strait Primer experiment using arrival time estimation and linearization," *J. Acoust. Soc. Am.*, vol. 118, pp. 2924–2933, 2005.

[12] G. C. Carter, "Time delay estimation for passive sonar signal processing," *IEEE Transactions on Acoustics, Speech, and Signal Processing*, vol. 29, pp. 463– 470, 1981.

[13] E. J. Hannan and P. J. Thomson, "Time delay estimation," *Journal of Time Series Analysis*, vol. 9, p. 2133, 1988.

[14] A. Piersol, "Time delay estimation using phase data," *IEEE Transactions on Acoustics, Speech, and Signal Processing*, vol. 29, pp. 471– 477, 1981.

[15] Y. Chan, J. Riley, and J. Plant, "A parameter estimation approach to time-delay estimation and signal detection," *IEEE Transactions on Acoustics, Speech, and Signal Processing*, vol. 28, pp. 8– 16, 1980.

[16] Y. Chan, J. Riley, and J. Plant, "Modeling of time delay and its application to estimation of nonstationary delays," *IEEE Transactions on Acoustics, Speech, and Signal Processing*, vol. 29, pp. 577–581, 1981.

[17] C. H. Knapp and G. C. Carter, "The generalized correlation method of estimation of time delay," *IEEE Transactions on Acoustics, Speech, and Signal Processing*, vol. 24, pp. 320–327, 1976.

[18] L. Bjørnø, *Underwater acoustics and signal processing.* D. Reidel Publishing Company, 1981.

[19] Z.-H. Michalopoulou and M. Picarelli, "Gibbs Sampling for time-delay and amplitude estimation in underwater acoustics," *J. Acoust. Soc. Am.*, vol. 117, pp. 799–808, 2005.

[20] C. K. Carter and R. Kohn, "On Gibbs Sampling for state space models," *Biometrika*, vol. 81, pp. 541–553, 1994.

[21] G. Casella and E. I. George, "Explaining the Gibbs Sampler," *The American Statistician*, vol. 46, pp. 167–174, 1992.

[22] A. Doucet, N. D. Freitas, and N. Gordon, *Sequential Monte Carlo Methods in Practice.* Springer, 2001.

[23] L. D. Stone, C. A. Barlow, and T. L. Corwin, *Bayesian Multiple Target Tracking.* Artech House Publishers, 1999.

[24] P. Gerstoft, "Inversion of seismoacoustic data using genetic algorithms and a posteriori probability distributions," *The Journal of the Acoustical Society of America*, vol. 95, no. 2, pp. 770–782, 1994.

[25] S. E. Dosso, "Quantifying uncertainty in geoacoustic inversion. 1. a fast Gibbs Sampler approach," *J. Acoust. Soc. Am.*, vol. 111, pp. 129–142, 2002.

[26] A. Tolstoy, "Linearization of the matched field processing approach to acoustic tomography," *The Journal of the Acoustical Society of America*, vol. 91, no. 2, pp. 781–787, 1992.

[27] S. E. Dosso and B. J. Sotirin, "Optimal array element localization," *J. Acoust. Soc. Am.*, vol. 106, pp. 3445–3459, 1999.

[28] W. Menke, *Geophysical Data Analysis: Discrete Inverse Theory.* Academic Press, 1989.

[29] A. Tarantola, *Inverse Problem Theory*. SIAM, 2005.

[30] R. Aster, B. Borchers, and C. Thurber, *Parameter Estimation and Inverse Problems*. Elsevier Academic Press, 2005.

[31] R. L. Parker, *Geophysical Inverse Theory*. Princeton University Press, 1994.

[32] E. Hensel, *Inverse theory and applications for engineers*. Princeton Hall, 1991.

[33] A. Tarantola, "Linearized inversion of seismic reflection data," *Geophysical Prospecting*, vol. 32, p. 9981015, 1984.

[34] G. C. Beroza and P. Spudich, "Linearized inversion for fault rupture behavior: Application to the 1984 morgan hill, california, earthquake," *Journal of Geophysical Research*, vol. 93, pp. 6275–6296, 1988.

[35] L. Jaschke, *Geohysical Inversion by the Freeze Bath Method with an Application to Geoacoustic Ocean Bottom Parameter Estimation*. PhD thesis, University of Victoria, 1997.

[36] P. Pignot and N. R. Chapman, "Tomographic inversion of geoacoustic properties in a range-dependent shallow-water environment," *J. Acoust. Soc. Am.*, vol. 110, pp. 1338–1348, 2001.

[37] B. Picard and E. Anterrieu, "Comparison of regularized inversion methods in synthetic aperture imaging radiometry," *IEEE Transactions on Geoscience and Remote Sensing*, vol. 43, pp. 218–224, 2005.

[38] D. E. Chauveau, A. C. M. Vanrooij, and F. H. Ruymgaart, "Regularized inversion of noisy laplace transforms," *Advances in Applied Mathematics*, vol. 15, pp. 186–201, 1994.

[39] P. C. Hansen, *Rank-Deficient and Discrete Ill-Posed Problems: Numerical Aspects of Linear Inversion*. SIAM, 1998.

[40] A. Tolstoy, "Haro Strait geometry (flat bottom)," *J. Acoust. Soc. Am.*, vol. 119, pp. 1388–1395, 2006.

[41] A. Tolstoy, "Haro Strait geometry (sloping bottom)," *J. Acoust. Soc. Am.*, vol. 120, pp. 1335–1346, 2006.

[42] E. A. Lehmann, "Particle Filtering approach to adaptive time-delay estimation," in *Proceedings of the International Conference on Acoustics, Speech, and Signal Processing, ICASSP-2006*, vol. 4, (Toulouse, France), pp. 1129–1132, 2006.

[43] J. J. Fuchs, "Multipath time-delay detection and estimation," *IEEE Transactions on Signal Processing*, vol. 47, pp. 237–243, 1999.

[44] G. C. Carter, "Time delay estimation for passive sonar signal processing," *IEEE Transactions on Acoustics, Speech, and Signal Processing*, vol. 29, pp. 463–470, 1981.

[45] J. E. Ehrenberg, T. E. Ewart, and R. D. Morris, "Signal processing techniques for resolving individual pulses in a multipath signal," *J. Acoust. Soc. Am.*, vol. 63, pp. 1861–1865, 1978.

[46] S. Geman and D. Geman, "Stochastic relaxation, Gibbs distributions, and the Bayesian restoration of images," *IEEE Trans. Pattern Anal. Machine Intell*, p. 721741, 1984.

[47] A. E.Gelfand and A. F. Smith, "Sampling-based approaches to calculating marginal densities," *Journal of the American Statistical Association*, vol. 85, p. 398409, 1990.

[48] A. E. Gelfand, S. E. Hills, A. Racine-Poon, and A. F. M. Smith, "Illustration of Bayesian inference in normal data models using Gibbs Sampling," *Journal of the American Statistical Association*, vol. 85, pp. 972–985, 1990.

[49] D. A. Sorensen, S. Andersen, D. Gianola, and I. Korsgaard, "Bayesian inference in threshold models using Gibbs Sampling," *Genetics Selection Evolution*, vol. 27, pp. 229–249, 1995.

[50] R. E. Kalman, "A new approach to linear filtering and prediction problems," *Transactions of the ASME - Journal of Basic Engineering*, vol. 82 (series B), pp. 35–45, 1960.

[51] J. V. Candy and E. J. Sullivan, "Ocean acoustic signal processing: A model-based approach," *J. Acoust. Soc. Am.*, vol. 92, p. 31853201, 1992.

[52] J. V. Candy, "Model-based signal processing," *J. Acoust. Soc. Am.*, vol. 119, pp. 2553–2553, 2006.

[53] E. A. Lehmann and R. C. Williamson, "Particle Filter design using importance sampling for acoustic source localization and tracking in reverberant environments," *IEEE Transactions on Speech and Audio Processing*, vol. 11, pp. 826–836, 2003.

[54] M. Orton and W. Fitzgerald, "A Bayesian approach to tracking multiple targets using sensor arrays and Particle Filters," *IEEE Transactions on Signal Processing*, vol. 50, pp. 216–223, 2002.

[55] F. Gustafsson, F. Gunnarsson, N. Bergman, U. Forssell, J. Jansson, R. Karlsson, and P. J. Nordlund, "Particle Filters for positioning, navigation, and tracking," *IEEE Transactions on Signal Processing*, vol. 50, pp. 425–437, 2002.

[56] B. Ristic, N. Gordon, and S. Arulampalam, *Beyond the Kalman Filter: Particle Filters for Tracking Applications*. Artech House, 2004.

[57] R. G. Brown and P. Y. C. Hwang, *Introduction to Random Signals and Applied Kalman Filtering*. John Wiley and Sons, 1997.

[58] R. J. Meinhold and N. D. Singpurwalla, "Understanding the Kalman Filter," *The American Statistician*, vol. 37, pp. 123–127, 1983.

[59] Z.Chen, "Bayesian Filtering: from Kalman Filters to Particle Filters, and beyond," 2003. Available at http://soma.crl.mcmaster.ca/ zhechen/download/ieee_bayesian.ps.

[60] Y. B. Shalom, X. R. Li, and T. Kirubarajan, *Estimation with Applications to Tracking and Navigation: Theory, Algorithms, and Software*. New York: Wiley, 2001.

[61] B. D. O. Anderson and J. B. Moore, *Optimal Filtering*. Prentice-Hall, 1979.

[62] S. Julier, J. Uhlmann, and H. F. Durrant-White, "A new method for nonlinear transformations of means and covariances in filters and estimators," *IEEE Transactions on Automatic Control*, vol. 45, pp. 477–482, 2000.

[63] A. Doucet and S. G. andn C. Andrieu, "On sequential Monte Carlo sampling methods for Bayesian Filtering," *Statistics and Computing*, vol. 10, pp. 197–208, 2000.

[64] A. Doucet, J. F. G. de Freitas, and N. J. Gordon, *Sequential Monte Carlo methods in practice*. New York: Springer-Verlag, 2001.

[65] A. Doucet, S. Godsill, and C. Andrieu, "On sequential Monte Carlo sampling methods for Bayesian filtering," *Statistics and Computing*, vol. 10, pp. 197–208, 2000.

[66] C. Andrieu, N. D. Frietas, A. Doucet, and M. I. Jordan, "An introduction to MCMC for machine learning," *Machine learning*, vol. 50, pp. 5–43, 2003.

[67] A. Doucet and A. Johansen, "A tutorial on Particle Filtering and smoothing: Fifteen years later," 2008.

[68] C. Hue, J.-P. L. Cadre, and P. Pérez, "Tracking multiple objects with Particle Filtering," *IEEE Transactions on Aerospace and Electronic Systems*, vol. 38, pp. 791– 812, 2002.

[69] C. Kreucher, K. Kastella, and A. O. HeroIII, "Multitarget tracking using the joint multitarget probability density," *IEEE Transactions on Aerospace and Electronic Systems*, vol. 41, pp. 1396– 1414, 2005.

[70] Y. B. Shalom, T. Kirubarajan, and X. Lin, "Probabilistic data association techniques for target tracking with applications to sonar, radar and EO sensors," *IEEE A&E Systems Magazine*, vol. 20, pp. 37–54, 2005.

[71] J. Vermaak, S. J. Godsill, and P. Perez, "Monte Carlo filtering for multi-target tracking and data association," *IEEE Transactions on Aerospace and Electronic Systems*, vol. 41, pp. 309–332, 2005.

[72] C. Hue, J. P. L. Cadre, and P. Perez, "Tracking multiple objects with particle filtering," *IEEE Transactions on Signal Processing*, vol. 38, pp. 791– 812, 2002.

[73] N. Chopin, "A sequential Particle Filter method for static models," *Biometrika*, vol. 89, pp. 539–552, 2002.

[74] M. Arulampalam, S. Maskell, N. Gordon, and T. Clapp, "A tutorial on Particle Filters for online nonlinear/non-Gaussian Bayesian tracking," *IEEE Transactions on Signal Processing*, vol. 50, pp. 174–188, 2002.

[75] N. J. Gordon, D. J. Salmond, and A. F. M. Smith, "Novel approach to nonlinear/non-Gaussian Bayesian state estimation," *IEE Proc. F, Radar and Signal Processing*, vol. 140, no. 2, pp. 107–113, 1993.

[76] J. Míguez, "Analysis of parallelizable resampling algorithms for Particle Filtering," *Signal Processing*, vol. 87, pp. 3155–3174, 2007.

[77] R. Douc and O. Cappé, "Comparison of resampling schemes for Particle Filtering," in *Proceedings of the 4th International Symposium on Image and Signal Processing and Analysis*, pp. 64 – 69, 2005.

[78] F. Daum and J. Huang, "Curse of dimensionality and particle filters," in *Proc. IEEE Aerospace Conf.*, 2003.

[79] Y. Zhou, P. C. Yip, and H. Leung, "Tracking the direction-of-arrival of multiple moving targets by passive arrays: algorithm," *IEEE Transactions on Signal Processing*, vol. 47, pp. 2655–2666, 1999.

[80] A. T. Alouani and W. D. Blair, "Technical notes and correspondence," *IEEE Transactions on Automatic Control*, vol. 38, pp. 1107–1110, 1993.

[81] W. D. Blair and G. A. Watson, "Tracking constant speed targets using a kinematic constraint," *IEEE Transactions on Aerospace and Electronic Systems*, vol. 38, pp. 233–238, 2002.

[82] F. Gustafsson, F. Gunnarsson, N. Bergman, U. Forssell, J. Jansson, R. Karlsson, and P. J. Nordlund, "Particle filters for positioning, navigation, and tracking," *IEEE Transactions on Signal Processing*, vol. 50, pp. 425–437, 2002.

[83] X. R. Li and V. P. Jilkov, "Survey of maneuvering target tracking, part i: Dynamic models," *IEEE Transactions on Aerospace and Electronic Systems*, vol. 39, pp. 1333–1363, 2003.

[84] W. Fong, S. J. Godsill, A. Doucet, and M. West, "Monte Carlo smoothing with application to audio signal enhancement," *IEEE Transactions on Signal Processing*, vol. 50, pp. 438–449, 2002.

[85] C. Andrieu and A. Doucet, "Joint Bayesian model selection and estimation of noisy sinusoids via reversible jump MCMC," *IEEE Transactions on Signal Processing*, vol. 47, pp. 2667–2676, 1999.

[86] J. R. Larocque, J. P. Reilly, and W. Ng, "Particle Filters for tracking an unknown number of sources," *IEEE Transactions on Signal Processing*, vol. 50, pp. 2926–2937, 2002.

[87] G. Castella and C. P. Robert, "Rao-blackwellisation of sampling schemes," *Biometrika*, vol. 83, pp. 81–94, 1996.

[88] Z.-H. Michalopoulou, "Multiple source localization using a maximum a posteriori Gibbs Sampling approach," *J. Acoust. Soc. Am.*, vol. 120, pp. 2627–2634, 2006.

[89] M. Wax and T. Kailath, "Detection of signals by information theoretic criteria," *IEEE Transactions on Acoustics, Speech, and Signal Processing*, vol. 33, pp. 387–392, 1985.

[90] H. Tanizaki, "Nonlinear and non-Gaussian state space modeling using sampling techniques," *Ann. Inst. Statist. Math.*, vol. 53, pp. 63–81, 2001.

[91] R. E. Helmick, W. D. Blair, and S. A. Hoffman, "Fixed interval smoothing for Markovian switching systems," *IEEE Transactions on Information Theory*, vol. 41, pp. 1845–1855, 1995.

[92] S. J. Godsill, A. Doucet, and M. West, "Monte Carlo smoothing for nonlinear time series," *Journal of the American Statistical Association*, vol. 99, pp. 156–168, 2004.

[93] C. F. Huang, P. Gerstoft, and S. Hodgkiss, "Uncertainty analysis in Matched-Field geoacoustic inversion," *J. Acoust. Soc. Am.*, vol. 119, pp. 197–207, 2006.

[94] Y. M. Jiang and N. R. Chapman, "Quantifying the uncertainty of geoacoustic parameter estimates for the New Jersey shelf by inverting air gun data," *J. Acoust. Soc. Am.*, vol. 121, pp. 1879–1894, 2007.

[95] S. E. Dosso and P. L. Nielsen, "Quantifying uncertainty in geoacoustic inversion. ii. application to broadband, shallow-water data," *J. Acoust. Soc. Am.*, vol. 111, pp. 143–159, 2002.

[96] M. K. Sen and P. L. Stoffa, "Bayesian inference, Gibbs' Sampler and uncertainty estimation in geophysical inversion," *Geophysical Prospecting*, vol. 44, pp. 313–350, 1996.